IEEE Access
Multidisciplinary : Rapid Review : Open Access Journal

Received 26 January 2024, accepted 22 February 2024, date of publication 4 March 2024, date of current version 8 March 2024.

Digital Object Identifier 10.1109/ACCESS.2024.3373188

RESEARCH ARTICLE

Fresh Properties and Autonomous Deposition of Pseudoplastic Cementitious Mortars for Aerial Additive Manufacturing

BARRIE DAMS[1], BINLING CHEN[1,2], YUSUF FURKAN KAYA[3,4], LACHLAN ORR[3,4], BASARAN BAHADIR KOCER[3,5], PAUL SHEPHERD[1], MIRKO KOVAC[3,4], (Member, IEEE), AND RICHARD J. BALL[1]

[1]Department of Architecture and Civil Engineering, University of Bath, BA2 7AY Bath, U.K.
[2]School of Mechanical Engineering, Beijing Institute of Technology, Beijing 100081, China
[3]Aerial Robotics Laboratory, Department of Aeronautics, Imperial College London, SW7 2AZ London, U.K.
[4]Laboratory of Sustainability Robotics, Swiss Federal Laboratories for Materials Science and Technology (EMPA), 8600 Dübendorf, Switzerland
[5]School of Civil, Aerospace and Design Engineering, University of Bristol, BS8 1TR Bristol, U.K.

Corresponding author: Barrie Dams (bd272@bath.ac.uk)

This work was supported in part by the Aerial Additive Manufacturing Project funded by the Engineering and Physical Sciences Research Council (EPSRC) under Grant EP/N018494/1, in part by the Royal Woolfson Society Fellowship under Grant RSWF/R1/18003, in part by the EPSRC Centre for Decarbonisation of the Built Environment (dCarb) under Grant EP/L016869/1, in part by the University of Bath Research Scholarship, and in part by the Imperial College Fellowship.

ABSTRACT Additive Manufacturing (AM) in relation to the construction industry is an emerging technology. However, ground-based AM on construction scales may be limited by the dimensions, reach and weight of the ground-based deposition platform. Aerial additive manufacturing (AAM) can revolutionise construction-based AM by employing multiple untethered unmanned aerial vehicles (UAV, known as 'drones') depositing material using miniature deposition devices. This study investigates aerial platform and cementitious material requirements for AAM and details development of structurally viable cementitious composite material with suitable rheological properties to demonstrate AAM as a novel aerial approach to complement ground-based activities. A synergistic combination of natural hydrophilic and partially synthetic hygroscopic polymeric hydrocolloids was developed in cementitious material to achieve optimal rheology properties in the fresh state. Analysis involved oscillation and flow tests, calorimetry, microscopy, computed tomography and mechanical tests. AAM application considerations focused on technical characteristics of UAV platforms, flight times, payloads and developed extrusion systems with optimal nozzle dimensions. Results demonstrate critical material parameters of 1700 kg/m^3 density, 4° phase angle, 1.1 kPa yield stress, $<$10 MPa complex modulus, and the ability to be processed through miniature deposition devices with 500 N force and 250 mA current. Material extrusions were realised using a custom-designed miniature deposition system which a UAV can carry and power. AAM will significantly impact automated construction by enabling new advances in aerial platform applications featuring multiple coordinated agents depositing bespoke material. This is particularly relevant to elevated or challenging construction conditions where an automated aerial approach can crucially reduce safety risks.

INDEX TERMS Aerial additive manufacturing, pseudoplastic cementitious material, rheology, unmanned aerial vehicles, 3D printing feasibility.

I. INTRODUCTION

Additive manufacturing (AM) has revolutionised automated production in sectors such as the medical, automotive

The associate editor coordinating the review of this manuscript and approving it for publication was Tao Liu.

© 2024 The Authors. This work is licensed under a Creative Commons Attribution 4.0 License.
For more information, see https://creativecommons.org/licenses/by/4.0/

and aerospace industries [1]. However, in the traditionally conservative construction industry [2], where construction methods have evolved to a minimal extent [3], the use of AM methods is still in a relative state of inception [4]. However, there has been some degree of growth because of the potential of AM to provide advancements in material efficiency, production efficiency, safety and a reduction in the quantity of waste material generated [5], [6], [7], [8] including growth in AM using concrete over the past decade [9].

The extrusion-based method of AM deposits suitably viscous material through a nozzle [10] to create an object in layers [11], therefore only using the exact amount of material required and no more. This contrasts with the subtractive method traditionally employed by the construction industry, which reduces a large block of material down to the required dimensions [12]. Considering the scale of a construction project, there is enormous potential to vastly reduce material wastage by utilising AM techniques over standard subtractive methods [13]. Increased automation on a construction project improves efficiency and increases productivity [14], [15], reduces costs [16], particularly those associated with labour [17]. This can also crucially reduce the risk of fatalities and injuries [13], [18], particularly in harsh or challenging environments [19], since the construction is an inherently dangerous and labour-intensive industry [20], [21]. Additionally, AM provides scope for greater architectural freedom [22] and bespoke design [23] at little extra cost, which in turn can promote innovation in design [10].

In traditional concrete construction practice, formwork contains freshly poured concrete. The absence of formwork in AM practice is central to the challenge of suitable cementitious material development [24]. The removal of formwork offers greater scope for bespoke architectural design [25]. However, this requires cementitious material, while in the fresh state, to possess appropriate rheological parameters [26], [27], combined with established hydration time-scales [28]. The absence of formwork also significantly reduces construction costs [16], [24]. Ground-based AM studies using 3D extrusion-printing principles have established parameters to characterise material while in the fresh state [10], [26], [29].

AM construction methods can be utilised in a pre-cast factory setting [30], fabricating parts off-site for subsequent transportation and assembly, or can take place entirely in-situ [10]. Investigations into the use of AM for construction have highlighted differing approaches. Large gantry-style frames, typically with three degrees of freedom and attached deposition equipment, can be considered suitable for standard design and bulk volumes [31] with low costs per unit [32]. Robotic arms possessing multiple degrees of freedom, either in the configuration of a large single robot [11] or a group, can realise more complex designs [31].

Ground-based in-situ printing requires favourable environmental conditions [29], with suitably level topography. The dimensions of the printed object are restricted by the dimensions and ensuing building envelope of the deposition system [33]. This is an issue when considering the height of a typical structure, with parts for multi-storey buildings requiring off-site prefabrication [32]. However, prefabrication also has drawbacks regarding the cost and logistical issues in creating and transporting customised components to the site [31].

An approach to addressing these issues would be introducing an aerial capability to automated in-situ construction, thus freeing a building project from ground and labour-based constraints. The aerial additive manufacturing (AAM) project proposes an innovative solution to bring aerial capability to in-situ AM by using a coordinated, communicating group of unmanned aerial vehicles (UAV). Each UAV is designed to carry an automated lightweight miniature deposition device, replete with a structural material, to create or repair structures in diverse and challenging environments [34], [35], [36], [37], [38]. AAM material development required considerable modification of traditional mortar mixes and different mix proportions to those featured in ground-based AM studies such as contour crafting [39], and concrete printing [22], [29].

The extrusion of structural material during controlled flight represents a paradigm shift in the use of UAVs in the construction industry, which previously had been limited to surveillance work [40]. Early studies of aerial robot deployment in construction have covered mainly the on-site assembly of prefabricated [41] or specifically designed components [42], ropes for tensile structuring [43], [44], [45], [46], and polystyrene prisms [41]. Recent studies have demonstrated real-world applications of discrete aerial additive manufacturing by assembling concrete blocks [47] and a reconfigurable structure of cyber-physical modules with onboard sensing and computing [48]. Even though these studies indicate novelties and improvements in scale, structural viability, and flexibility, the design of those particular elements necessitates significant labour, cost, and a certain amount of lead time for the final assembly. These deficiencies heavily lessen the power of discrete AM and orient the research direction towards continuous AM.

Fig. 1 illustrates the conceptual vision of AAM with a small swarm of UAVs extruding a pseudoplastic cementitious material. It has been demonstrated that a cementitious mortar with suitable rheological properties and an appropriate balance between workability and buildability can be extruded by multiple coordinated flying UAVs in a complex trajectory and to a high level of precision [38]. The aerial approach would be particularly advantageous when working at height or in a post-disaster reconstruction environment with difficult ground conditions [35].

This study builds upon AAM project work [37] by examining the differences between on-site aerial and off-site ground-based AM requirements, identifying suitable aerial platforms while detailing the refined development of a novel pseudoplastic cement-based composite material with suitable rheological properties for AAM. With material development,

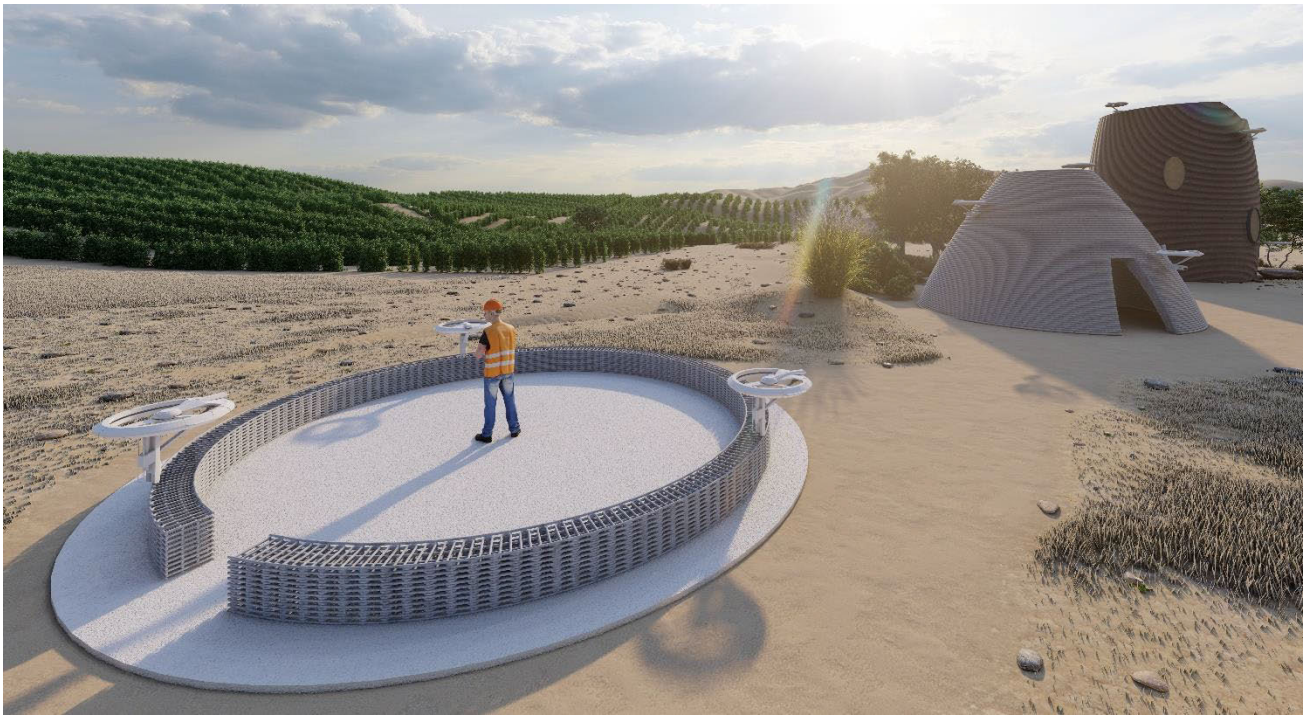

FIGURE 1. The conceptual representation of aerial additive building manufacturing (AAM) with multiple coordinated unmanned aerial vehicles (UAV) extruding a suitable pseudoplastic mortar in a customised continuous curve printing path.

there is an emphasis upon the addition of polymeric rheology modifying admixtures (RMA) to enhance cohesion, stability and water retention [49] within fresh mix open-times. The importance of identifying a UAV platform with appropriate technical characteristics and miniaturising the deposition process for AAM in relation to ground-based methods is highlighted. In addition, extrudability and pumpability are amalgamated into the encompassing term 'workability'. Crucial to material development suitable for AAM is recognising the inherent trade-off between workability and buildability (the ability of an extruded material to retain shape and structure while in the fresh state), which requires contrasting rheological characteristics. The former requires low viscosities and liquid-like behaviour, while the latter requires high viscosities and solid-like behaviour to resist deformation from subsequently deposited layers. Freshly mixed material is required to pass through a light, miniaturised deposition system appropriate for carriage on a flying UAV. The deposition system must process the material without adversely interfering with power delivery capabilities or the lateral precision of a UAV while following an architecturally informed programmed trajectory. Extruded material should also be sufficiently rigid to resist downwash effects resulting from UAV propeller rotation.

A two-stage material formulation strategy is presented. In this study, two mixes first focus on buildability, and subsequently, three bespoke mixes focus on workability in conjunction with the development of a miniature deposition device and nozzle design. UAV platform options are evaluated for technical suitability with AAM material extrusion. Material tests encompass a wide range of experiments to ascertain an indication of suitable material properties for on-site AAM in accordance with the capabilities of the aerial platform. Tests in this study include material settlement, rheology, calorimetry and microstructure, along with optimisation of nozzle design and dimensions for material extrusion from miniature deposition devices.

II. EXPERIMENTAL METHODOLOGIES

A. AERIAL PLATFORM CONSTRAINTS EVALUATION

Aerial systems represent a class of open-loop unstable systems that present unique control challenges. These challenges are further compounded by the underactuated nature of the system, where the number of states exceeds the available control inputs. To tackle these complexities, considering cascaded or hierarchical control architectures becomes necessary, enabling the implementation of control loops operating at different frequencies and facilitating controller designs tailored to specific cycles. For applications such as AAM, which involve close flight proximity to objects and the environment, the system must maintain stability amidst reaction forces, aerodynamic reflections, and potential friction effects. Furthermore, the dynamics of the propellers change when operating in close proximity to the surroundings [50]. This proximity results in an increased rotor wake, leading to elevated propeller velocities and the emergence of the ground effect, which generates additional

repulsion forces from the ground. Additionally, material deposition during mid-flight introduces variations in the mass distribution, further emphasizing the need for adaptability in the overall system design to address these challenges.

Recent investigations have explored the utilisation of surface friction to enhance the precision of printing [51], yielding promising results with reported position accuracy in the range of 4 mm and printing precision of 1 cm. However, the relatively lower printing precision, particularly in corners, can be attributed to the flight dynamics of the aerial platform for the given trajectories, which result in material accumulation at these corner points. The AAM platform is a coupled six-degrees-of-freedom system that is under-actuated using four propellers. To mitigate possible yaw moments induced by the propellers, pairs of motors on each axis rotate in opposite directions with equal power. This configuration allows quad-rotors to adjust their position along the Z-axis easily by powering up all the motors. However, movement in the other two axes necessitates the speeding up of one set of rotors while simultaneously slowing down the other set [52]. Fig. 2 showcases the dynamics of UAV flight and illustrates the frame and movements of a quadrotor UAV. Combining insights from existing literature and conducting experimental UAV flights, a comprehensive evaluation of the differences between ground-based and aerial-based platforms is undertaken, highlighting the constraints specific to aerial systems.

B. DEPOSITION DEVICES

This study used two deposition device designs suitable for AAM as illustrated in Fig. 3 (adapted from the AAM project deposition device and delta stabilising robot design [38]). The 60 ml cartridge design accommodated two cartridges and was initially developed for systems requiring two liquid components, such as polyurethane foam [53]. The system could also function using one cartridge powered by a 6 V DC 298:1 micro metal gear motor and was used during initial pseudoplastic cementitious material development focusing upon mix buildability (Fig. 3*o*-u). The larger device in the principal image (Fig. 3*a*-n) employed a 310 ml cartridge powered by a 12 V motor and was developed to provide an up-scaled, more powerful deposition system capable of holding more material while being appropriate for the power and payload capabilities of the UAV platform [38]. Both designs used a powered descending plunger to push the material out of the cartridge (rather than an auger-based design) due to the rheology modifying admixtures used in material mixes.

During the study, the 60 ml capacity device was manoeuvred in three-dimensional space during laboratory experimentation by a Dobot Magician multi-functional robotic arm, with four degrees of freedom, and also by hand. The 310 ml capacity device nozzle was manoeuvred by hand. The tip of the 310 ml cartridge is connected by a length of 8 mm diameter flexible plastic tubing to the nozzle, which is located between universal joints at the base of a delta arm robot which attaches to a flying UAV. An additional tapering 3D-printed plastic component is placed into the 310 ml cartridge (Fig. 3*l*) to provide a sloping plane for the material to pass through the cartridge tip and into the tubing.

Deposition device specifications are shown in Table 1. When full of material, the total mass of both devices is within the 1 kg payload limit of a typical flying UAV. 310 ml cartridges were considered to have a volume of 202 ml in practice to allow for inserting a 3D-printed tapered component at the base of the cartridge and plunger insertion at the top. Similarly, 60 ml cartridges were considered to have a practical capacity of 50 ml due to the drilling of a hole in the side of the cartridge to allow injection of re-filling material by a supply cartridge (as seen in Fig. 3*r*,t).

Two nozzle designs were used during this study. An 8 mm diameter circular outlet was used with the automated deposition devices due to the current lateral stability levels of the yaw of the flying UAV platform rotating about its axis. For manually controlled extrusion, 3D-printed plastic components with 20 mm x 5 mm and 15 mm x 5 mm rectangular apertures were attached to the tip of a 60 ml cartridge (Fig. 3*s*) to compare ease of deposition with circular nozzle extrusion.

The volumetric flow rate Q within deposition devices can be calculated using the equation

$$Q = VA \tag{1}$$

where V is the mean material flow velocity and A is the cross-sectional area of the cartridge.

TABLE 1. Deposition device specifications.

Specification	310 ml device		60 ml device	
Cartridge internal diameter	47	mm	27	mm
Cartridge full height	213	mm	130	mm
Cartridge theoretical volume	310	ml	60	ml
Cartridge practical volume	202	ml	50	ml
DC brushed motor	12	V	6	V
Circular nozzle diameter	8	mm	8	mm
Circular nozzle area	50.3	mm^2	50.3	mm^2
Printing velocity	10	mms^{-1}	3.3	mms^{-1}
Printed volume/second	0.5	mls^{-1}	0.165	mls^{-1}
Cartridge flow velocity	0.294	mms^{-1}	0.265	mms^{-1}
Cartridge flow rate Q	510	mm^3s^{-1}	152	mm^3s^{-1}
Tube length	560	mm	-	-
Tube volume	28.2	ml	-	-
Tube flow velocity	4.44	mms^{-1}	-	-
Tube flow rate Q	223	mm^3s^{-1}	-	-

C. MATERIAL STRATEGY

Rheological modifying admixtures (RMA) were required to develop mortars with low segregation and provide a suitable balance between workability (defined in this study as the ability of a material to be processed by a miniaturised deposition system) and buildability (defined as the ability of a material to retain shape post-extrusion and accept subsequent layers without excessive deformation). Different types of

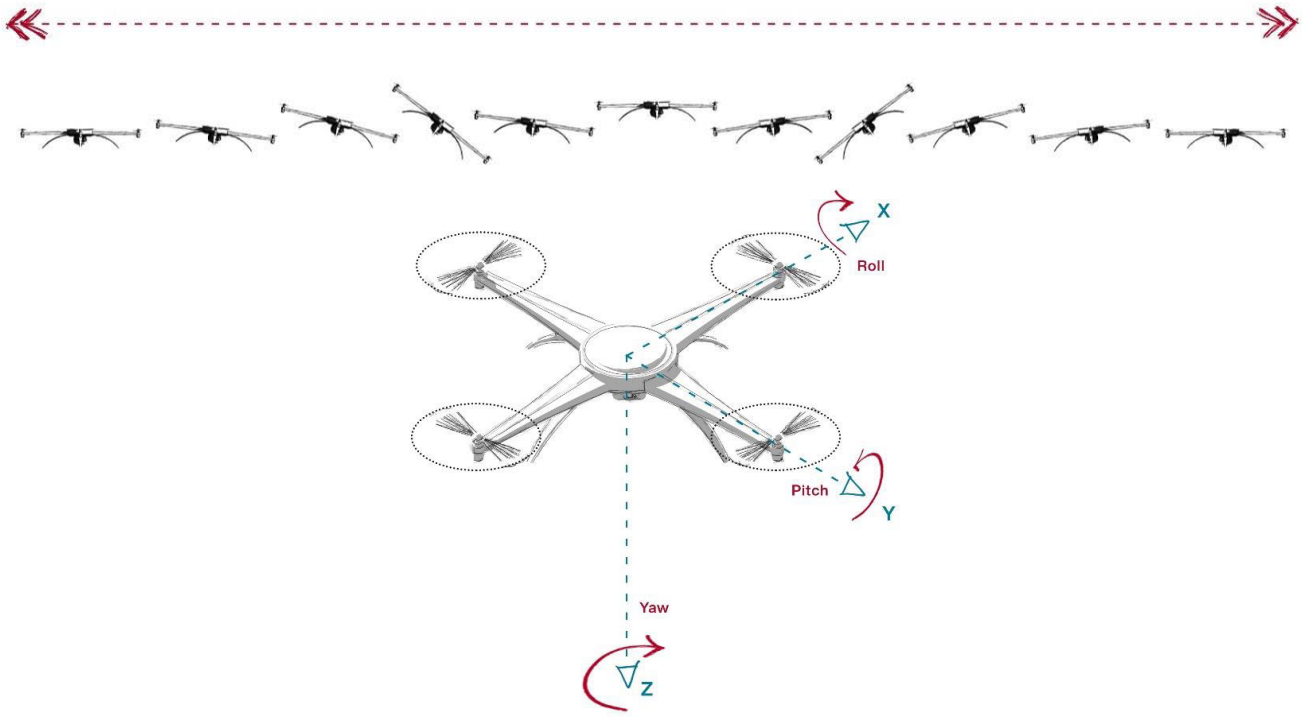

FIGURE 2. Quadrotors' flight dynamics along a movement in the X or Y axis (above) and an example of quadrotor frame (below).

microfibres for AAM mixes have been investigated by the authors [54]. This study focuses on developing pseudoplastic hydrocolloids in AAM mortars and does not include fibres in the fresh mixes. Pseudoplastic (shear-thinning) material is highly appropriate for a small, lightweight deposition system. The material should possess low viscosity while subjected to stresses within the components of the deposition system yet rapidly increase in viscosity and possess a suitable yield stress once deposited and in a state of rest.

A further consideration is whether to use fresh mixes' rheological properties (while consistent within the open time) to retain structure and shape following deposition or use accelerating admixtures to promote fast curing following deposition. Preliminary tests revealed that the open time of developed cementitious mixes rheologically suitable for AAM can be considered 120 minutes. The loading of material into an empty cartridge, the attachment of a full cartridge to a deposition device, and the launching, piloting, and global coordination of the UAV carrying a deposition device are precise and extensive procedures. If a technical issue is encountered, sufficient open time allows for a problem to be identified and rectified while the material still retains workability within a loaded cartridge. An accelerating admixture could be included as a constituent at the mixing stage or administered immediately before deposition. The former approach would reduce the operation window, risking wasting a cartridge full of material in the event of a technical issue. The latter approach would require either a significant deposition device adaptation to administer an accelerating agent to the mix immediately prior to deposition or a second accelerator-administering UAV. Additionally, the effectiveness of accelerating admixtures may be mitigated or negated by the potential retarding effects of pseudoplastic RMAs with microstructures of polymeric chains such as cellulose ethers [55]. Therefore, considering potential retardation effects and the operational benefits of a faster, streamlined mix-manufacturing operation, it was decided in this study not to use accelerating admixtures and instead focus on developing fresh mixes with suitable open-time rheological properties.

D. MATERIAL CONSTITUENTS

Fresh cementitious-based material suitable for AAM should possess an appropriate balance between workability and buildability. Hydrated material still needs to possess structurally viable strength, despite the requirement to reduce material density below typical mortar levels of $\approx$2000+ kg/m^3 for AAM [38]. Binding materials, additives and admixtures can contribute to either buildability, workability or both, with varying degrees of impact upon strength. Fig. 4 schematically illustrates constituents investigated in this study, along with the particle size distributions of fine aggregate used.

This study used Dragon Alfa CEM I 42.5 R Portland cement with a particle size of 5 - 30 μm and bulk density 900 - 1500 kg/m^3 as the base binding constituent. The chemical composition of the CEM I, determined by Rietveld quantitative phase analysis, is shown in Table 2.

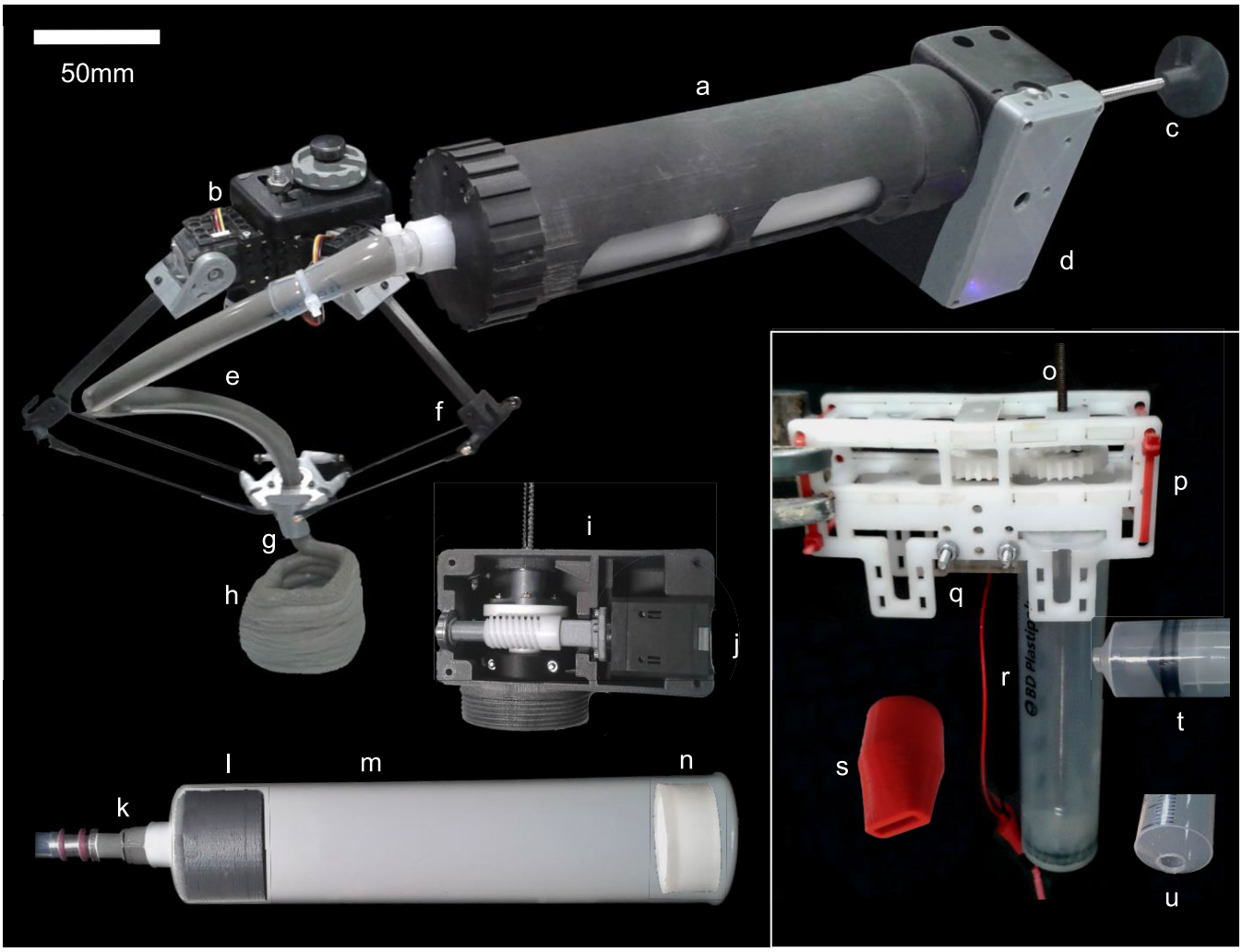

FIGURE 3. Two deposition devices developed for AAM - 310 ml capacity device (principal image) and 60 ml device (bottom-right partition): a) 310 ml cartridge casing and seal. b) Delta robot servomechanism. c) Threaded rod attached to the plunger. d) Gearbox casing. e) 8 mm diameter flexible tubing connecting cartridge and nozzle. f) Delta stabilising robot. g) 8 mm diameter circular nozzle. h) Multiple layer extrusion. i) Gearbox. j) 12 V metal gearmotor. k) Metal components securing tubing to the cartridge. l) 3D printed component with tapering interior. m) 310 ml capacity cartridge. n) Plunger. o) Threaded rod attached to the plunger. p) Gearbox and casing. q) 6 V micro metal gear-motor. r) 60 ml capacity cartridge. s) 3D printed rectangular nozzle attachment. t) Refilling cartridge. u) 8 mm diameter nozzle. (Principle image adapted from the AAM deposition device and delta robot design [38].

TABLE 2. Rietveld quantitative phase analysis of the chemical composition of Dragon Alfa CEM I 42.5 R Portland cement shown as a percentage by weight.

CEM I Phase	% by wt.
Dicalcium silicate C_2S	14.6
Tricalcium silicate C_3S	71.5
Tricalcium aluminate C_3A	7.27
Tetra-calcium aluminoferrite C_4AF	4.46
Calcium sulphate phases	2.16

Binding additives investigated were EN 450 N grade type-F pulverised fuel ash (PFA), supplied by Cemex, with a bulk density 800 - 1000 kg/m^3, particle size <45 μm, and silica fume supplied in powder form by FerroPem, France with a bulk density of 200 kg/m^3 and mean particle size of 0.2 μm. PFA, a by-product of the coal industry [56], was expected to aid workability, possessing a microstructure of smooth, rounded particles [26], in addition to contributing to the strength of mixes [56]. Constituents which contribute to higher-performance strength, such as silica fume and silica flour [56], were expected to contribute to buildability, with the small (generally below 0.1 μm) particles filling voids in material such as ordinary Portland cement type 1 (CEM I) and sand [26].

Coarse aggregate can be considered unsuitable for miniature AAM deposition devices, but fine aggregate with particle sizes of <2 mm diameter is feasible. The fine aggregate used in this study consisted of angular-particle and smooth-particle sand. Angular-particle sand (supplied by Jewsons, UK, product number AGSTB003) was kiln dried at a temperature of 105°C for twenty-four hours prior to sieving

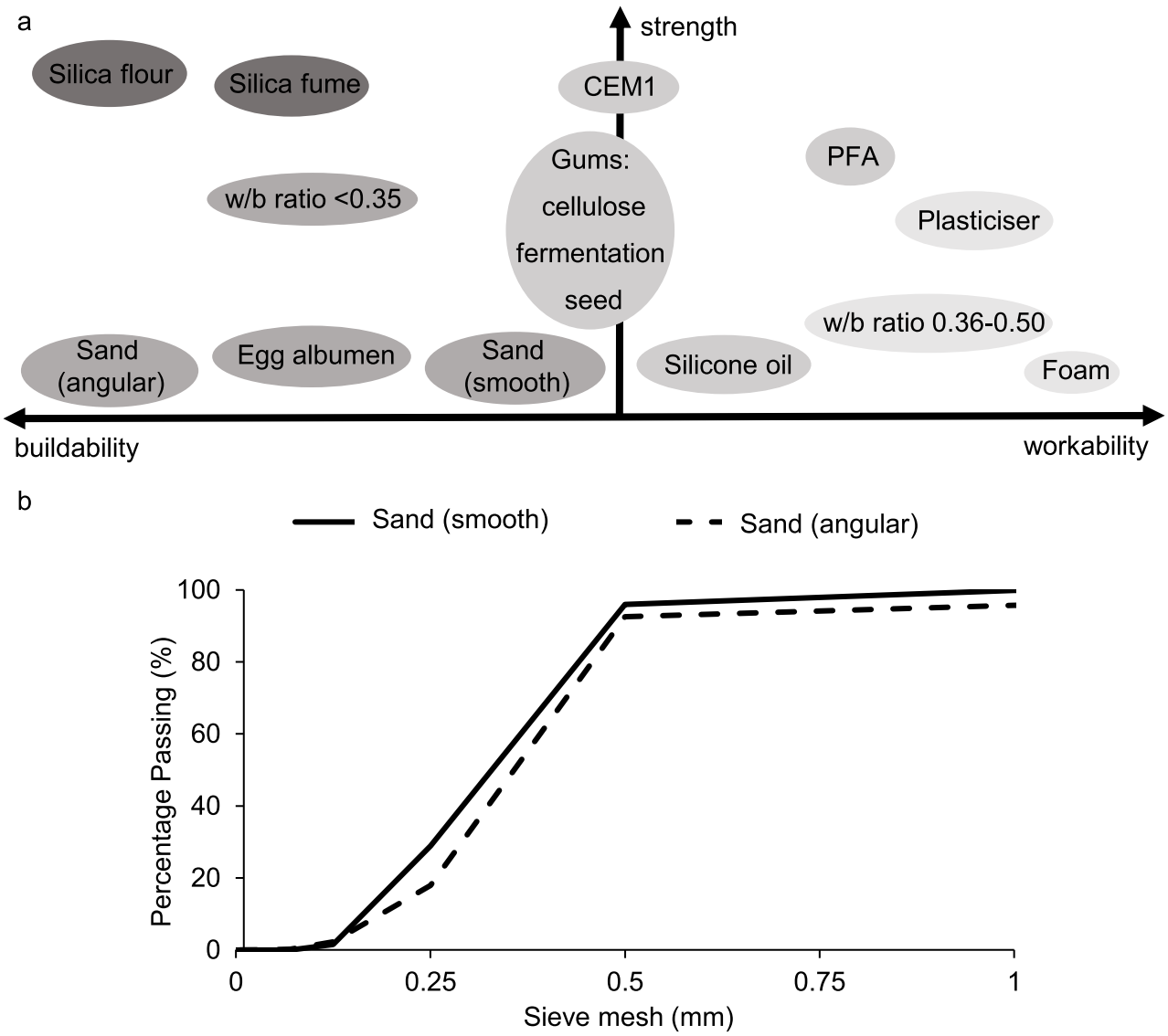

FIGURE 4. Constituents with particle distribution properties investigated for AAM. a) Schematic contribution to material properties' workability, buildability, and strength. b) Particle size gradation of fine aggregates.

and possessed a loose dry density of 1600 kg/m^3. Contrasting with angular to sub-angular particle sand, which has a broad particle distribution and generally larger particles creating voids for smaller particles to fill (thus aiding buildability), sand designed for use in sporting or outdoor recreational applications has generally smoother-surfaced particles and was also used in this study. The smooth sand (supplied by British Playsand, UK, product number 365/0574), was also kiln dried at a temperature of 105°C before use for twenty-four hours and possessed a lower dry density of 1450 kg/m^3. Fig. 4*b* shows the particle gradations attained by twenty minutes of mechanical sieving for the two types of sands.

Foaming agents, silicone oil, and hydrocolloids were all investigated as RMAs, both in isolation and combination, to modify the rheology of the mix and assess potential synergistic effects. Mixes required a binding, water-retaining agent to prevent bleeding and the ensuing build-up of fine-aggregate zones around the tip of the deposition cartridge as the material passed through, potentially causing blockage [57]. Mix formulation was informed by the behaviour of pseudoplastic materials such as paint, which requires low viscosity during application and high viscosity once applied and at rest [58].

Albumen-based foam was trialled alongside a cellular lightweight concrete foaming agent manufactured by EAB Associates, with the latter being more effective. When mixed at a concentration of 3% agent to 97% water, this product produced a foam of stiff-peak consistency in 15 seconds, which can be added to slurries. The foaming agent could not

be combined with silicone oil, as the latter possesses anti-foaming properties [59]. During trial mix formulation, it was discovered that EAB Associates foaming agent needed to be used in much smaller quantities to achieve the same effect on workability as silicone oil.

Hydroxyethyl methyl cellulose (HEMC), a synthetic hygroscopic compound [60] chemically derived from cellulose [61], was identified as a potentially suitable RMA. A pseudoplastic hydrocolloid, the addition of cellulose ethers are established in dry-mix mortars used for renders, tile adhesives and self-levelling applications [62], [63], [64], [65]. It is noted for viscosity modification [65], contribution to mechanical strength [66] and particularly water retention, via the mechanism of water sorption and the formation of water-retaining polymer networks within cementitious matrices [64].

The chosen plasticiser to provide further pseudo-plasticity was Adomix Adoflow S. This is a lignin-based plasticiser, working via the mechanism of electrostatic repulsion, where the polymeric molecule chains cover the cementitious binder particles and impart a repelling negative charge. This is the same mechanism used by naphthalene-based superplasticisers [67], and it has been noted that these exhibit shear thinning properties [68]. Conversely, polycarboxylate-based superplasticisers, working by the mechanism of steric stabilisation [69], can impart shear thickening properties into material [68].

E. MIX MANUFACTURE

Mixes were created in the laboratory using the following method:

1) Dry constituents - cementitious binder of CEM I and PFA, fine aggregate and hydrocolloids - were hand-mixed.
2) Water and plasticiser were mixed and poured evenly over dry constituents.
3) An automated mixer beater was activated for three periods of 30 seconds of planetary motion at high speed.
4) Separately, the foaming agent was added to water and mixed to a stiff-peak consistency.
5) The foam was then added to the mix and underwent two mixing periods for 10 seconds on a slow setting.

Mixes not containing foaming agents followed steps 1 - 3 only.

The temperature of the laboratory environment during mix-manufacturing was 20°C ±3°C, and the water added to dry constituents was 16.5°C ±2°C.

F. AXIAL FORCE AND POWER REQUIREMENTS

To discover the axial force required for a deposition device plunger to push a fresh mix through a deposition system, a rig was constructed as shown in Fig. 5*b*. Displacement-controlled force was applied at a constant rate of 5 mm/minute upon a plunger using a 50 kN Instron Universal 2630-120/305632 device.

Compressive stresses experienced by the fresh mixes while passing through a cartridge may be calculated using:

$$\sigma = \frac{F}{A} \tag{2}$$

where F is the axial force required and A is the cross-sectional area of the cartridge (as shown in Table 1).

To obtain the power required to process the mixes through miniature deposition systems, freshly mixed material was loaded into a cartridge and extruded, with the location of the nozzle in a three-dimensional space controlled by a robotic arm to simulate automated UAV movement (the 60 ml capacity device as shown in Fig. 5*a*) and by hand (the 310 ml capacity device). The power supply voltage was maintained at a constant 6 V for the 60 ml device and 12 V for the 310 ml device. A more buildable, viscous mix was expected to require greater current to be drawn from the power supply for successful extrusion.

G. MATERIAL DEFORMATION

Following extrusion, the deformation scenario of layer settlement affects the structure of fresh material. Layer settlement, which can be tested to quantify the stability of extruded material [70]. To investigate layer settlement, explicitly defined in this study as the extent to which a freshly extruded bead of material might compress under the weight of subsequently added layers, 8 mm diameter beads of mixed material were extruded onto steel plates to a length of 100 mm at 5 minute intervals. They were compressed at a 2 mm/minute rate by an upper steel plate fixed to the Instron Universal device, as shown in Fig. 5*c*-d. The tests were conducted over the material open period of two hours.

H. RHEOLOGY—OSCILLATION AND FLOW

Rheological tests were performed to quantify the pseudoplastic and viscoelastic properties of the mixes. Tests were conducted on a TA Instruments DHR2 rheometer at a constant temperature of 25°C. Oscillatory tests used disposable aluminium flat plates with a 40 mm base plate and 25 mm diameter upper plate. Flow tests used steel cross-hatched 40 mm base plate and upper plate to minimise slippage at greater shear rates. A 1000 μm geometry gap was used in all rheology tests, and material was placed upon the base plate immediately following mixing.

Displacement-controlled oscillation tests were conducted over two hours, representing the open time of the fresh material. An angular velocity of 5.0×10^{-5} radians per second ensured the material remained within the linear viscoelastic region. Frequency was maintained at 1 Hz. Tests quantified the rigidity of the mixes, with the complex modulus G^* parameter, consisting of:

$$G^* = G' + G'' \tag{3}$$

where G' is the solid-like behaviour component, storage modulus (recoverable elastic deformation as a result of energy storage), and G'' is the liquid-like behaviour component, loss

FIGURE 5. Robotic arm, axial force and material deformation tests. a) Robotic arm manipulating a 60 ml capacity device printing a fresh mix. b) Axial force test rig with direction of force indicated. c,d) Material deformation test rig shown with direction of uniformly distributed load indicated (c) and evaluating the settlement of an 8 mm diameter bead of extruded fresh material (d).

modulus (non-recoverable deformation due to viscous flow, resulting in dislocations in the micro-structure). The complex modulus G^* is calculated by:

$$G^* = \frac{G'}{\cos\delta} \tag{4}$$

where δ is the phase angle, further quantification of solid-like or liquid-like behaviour in the fresh material. A δ value, ranging between 0° (an ideal solid) and 90° (an ideal liquid) may be calculated as:

$$\delta = \tan^{-1}\frac{G''}{G'} \tag{5}$$

Secondly, stress-controlled flow tests were conducted at shear stresses ranging from 300 Pa to 3000 Pa to quantify pseudoplastic behaviour with the relationship between applied shear stress $\dot{\gamma}$ and resulting viscosity η and yield stress. The greater the decrease of η in relation to increased stress, as the material would be subjected to while progressing through the deposition systems, the greater the suitability of the mix for AAM.

The flow resistance R encountered by fresh material while in the cartridge and tubing can be calculated as:

$$R = \frac{8\eta L}{\pi r^4} \tag{6}$$

where η is the viscosity of the material in the cartridge or tubing, L is the length, and r is the radius of the cartridge or tubing.

I. CALORIMETRY

Calorimetry tests were conducted on fresh mixes with and without HEMC over 48 hours to determine how the cellulose-based hydrocolloid affected the heat evolution rate of the exothermic hydration reaction. 40 g samples of material were placed into sealed containers immediately after mixing and placed into a Calmetrix I-Cal 4000 high precision isothermal calorimeter with chambers maintained at 20°C.

J. MATERIAL MICROSTRUCTURE

The particle sizes and surfaces of the constituents and microstructure of 28-day cured mixes were examined using scanning electron microscopy (SEM). Samples were coated in a 10 nm layer of gold to prevent charging and increase signal-to-noise ratio and subsequently analysed using a JEOL SEM6480LV microscope.

K. X-RAY COMPUTED TOMOGRAPHY (CT)

The 3D structures of three selected printing trajectory designs, a wall (adjacent lines), an alternating 'ruffle' design and a continuous curve design, were investigated using x-ray computed tomography (CT). Previous tests by the AAM project had used these trajectory designs to demonstrate the versatility of the developed pseudoplastic material and the lateral precision capabilities of AAM material extrusion during flight [38]. The CT scans were measured using a Nikon XT H 225 ST model machine and conducted using

65 kV, an exposure rate of 1.5 seconds and 50 μA x-ray beam output. The obtained data files were subsequently analysed by using VGStudioMAX software.

III. RESULTS AND DISCUSSIONS

A. EVALUATION OF A SUITABLE AERIAL PLATFORM

Among AM research studies, AAM brings a different perspective by deploying aerial vehicles with a robotic manipulator to produce large-scale structures with additive manufacturing methods. This novel production method facilitates multi-agent parallel additive manufacturing with an unrestrained build envelope in hard-to-reach zones. This will allow maintenance tasks such as crack repair [71] to be performed at height without scaffolding or supporting infrastructure and free-form construction. AAM complements the limitations of ground-based systems and holds enormous potential and promise for robotic construction. Table 3 summarises the advantages and disadvantages of comparing ground-based robotic systems and aerial platforms in construction tasks.

Furthermore, the design of the aerial platform and extrusion mechanism is as important as the flight dynamics. The design difficulties related to the use of an aerial platform in continuous additive manufacturing tasks cover the positioning of the extrusion mechanism and nozzle, potent interaction with the construction surface, minimisation of structural vibrations and aerodynamic perturbations on the built structure caused by the aerial flow and propellers' downwash, and the scale optimisation of the overall system.

To clarify, flight dynamics can easily be disrupted by any change in the alignment of the centre of gravity. For that reason, to achieve higher printing accuracy, the positioning of the extrusion mechanism and nozzle should be in balance with the aerial platform's centre of gravity (CoG). Moreover, a certain distance between the nozzle and the propellers' level should be secured to decrease the downwash effect, which may cause the extruded material to scatter around. The general approach against these perturbations is using a manipulator [72], [73]. However, a unique way of re-compensating the negative effect of the aerial platform can be the deployment of multi-directional thrust systems [74]. In the current AAM framework, a parallel manipulator is used, which is added to the drone body to isolate vibrations and oscillations caused by the aerial platform's behaviour and minimise the effect of the downwash generated by the propellers. Another critical aspect of AAM is the dimensions and properties of the nozzle. The narrower the nozzle diameter, the greater the print length and resolution that can be achieved with each cartridge of fresh material. However, this will decrease the precision tolerance of the overall system and place extra importance on the lateral stability of the extrusion device while depositing fresh material. After a certain threshold, as the system cannot provide that clarity, errors such as breaking during the printing will occur. Furthermore, in an AAM application, a few practical aspects could be considered. An example of a hardware-based approach would be covering the area around the nozzle with a sheet of material to minimise the effect of the downwash generated by the propellers. The need to address downwash would also be reflected in the material development strategy, with extra emphasis being placed upon cementitious material possessing suitable rheology parameters and a yield stress sufficient to provide resistance to deformation due to downwash while in the fresh state.

Another significant constraint of the aerial platforms is their heavily bounded flight times and payload capacities [34]. This strictly defines the maximum amount of material printed within a single flight. While it is possible to solve the problem of carrying capacity and limited

TABLE 3. Advantages and disadvantages of different robotic construction methods.

Method	Advantages	Disadvantages
Off-site Ground-based Platforms	- High-precision rate in various construction tasks. - High-quality end product because of high standardisation. - Reduced risk of work-related health problems and increased safety. - Reduced disruption in the local neighbourhood of the construction site.	- Low flexibility in design and manufacturing. - Low scalability. - Predefined and restricted build envelope. - High transport volume causes an increase in CO2 emissions and costs. - High dependability on terrain conditions. - The necessity to complete the structure design in advance. - The necessity of lead manufacturing time. - Lack of access to extreme environments and conditions. - Not supporting agile applications like inspection, repair or manufacturing in remote and hard-to-access places.
On-site Aerial Platforms	- High access to extreme environments and conditions. - High and relatively unrestricted build envelope. - Ease of scalability. - Low transportation costs. - Agnostic to ground terrain conditions. - Ease of intervention during construction. - Ease of use in agile construction tasks. - No lead construction time is required.	- Relatively low precision rate in various construction tasks. - Low payloads and mission duration constraints. - High iteration in large-scale construction. - High sensitivity against air conditions and wind. - Low-quality end product because of insufficient developments in hardware and software.

energy by scaling up the aerial vehicle, it should not be forgotten that this will compromise safety and mobility. The negotiation between these two necessitates an effective scale optimisation. Two basic approaches are presented here. The first is developing and producing a platform suitable for the target task, and the second is choosing and adapting the most suitable off-the-shelf platform. Recent work on the first approach of aerial platform optimisation is the compact coaxial tri-rotors developed by Orr et al. [75], specially designed for aerial construction and repair operations. In addition, there is further interest in aerial perching to extend operation time [76], battery-tethered aerial vehicles [77], more efficient battery technologies [78] and efficient mission planning [79] in this context.

If the project time is restricted, selecting an 'off-the-shelf' aerial platform might be a better way to proceed. For the research presented herein, the unmanned aerial vehicle will be required to withstand the weight of the deposition device under 1 kg during flight. In addition, according to the figures in Table 4, the total printing time of a singular layer of material may be under 10 minutes. Therefore, the endurance of the flying vehicle can be kept within 20 to 30-minute intervals to allow for small-distance flying and printing time.

Table 4 displays the technical characteristics of seven off-the-shelf UAVs to be considered for aerial additive manufacturing using the deposition devices mentioned above. It is worth noting the maximum flight time of a flying device is determined with no payload; as the mass added onto the main body increases, the endurance will decrease. From this, the vehicles that meet both payload and endurance criteria set above and therefore suitable for the mission mentioned above are Aurelia X6 standard, Hercules 10 or Hercules 20 with a flight time while loaded with 1 kg of a payload of over 20, 30 and 37 minutes, respectively.

TABLE 4. Technical characteristics of off-the-shelf UAV's.

UAV	Payload (Kg)	Max. flight time (mins)	Endurance with 1 kg payload (mins)	Source
Aurelia X6 Standard	5	30	>20	[80]
Tarot 650 v2.2	1.5	25	10	[81]
SplashDrone 3+	1	30	(-)	[82]
Fisherman	2	30	15	[83]
SplashDrone 4	2	30	15	[84]
Hercules 20	15	40	37	[85]
Hercules 10	7.5	35	20	[86]

This scale optimisation is also a highly significant topic for collective robotic construction [87]. The use of a swarm of UAVs to manufacture buildings enables greater scalability, increase the speed of production, and improve the robustness of the methodology since the loss of an agent won't affect production and can be easily replaced. Bigger UAVs will lead to less task parallelization. Even though the UAVs would have a higher payload and flight endurance, there should be an optimum number of agents with an optimum scale to get the full potential of AAM realised. Zhang et al. [38] demonstrated a dry flight of three UAVs working collaboratively to build the light trace of a dome structure. However, the collective robotic construction software framework for UAVs is a topic of ongoing wider research endeavours [88].

Sub-millimetre precision is a hard-to-reach range for aerial platforms and it poses a significant challenge for aerial construction tasks. Therefore, aerial construction literature heavily uses motion capture systems that can manage this precision level. However, these systems are still only stepping stones towards the potential promise of AAM for on-site tasks. To overcome this problem, multi-sensor fusions, for example, a GPS module with a SLAM camera or LIDAR, can be used for more precision in localisation [89], [90], [91].

After handling the localisation, mission planning should be dealt with for multi-agent AAM. This has been investigated [92]; however, another challenge of lack of physical reference is additionally introduced in the case of aerial platforms. Moreover, the time aspect is an extra dimension in mission planning over ground-based systems' two or three dimensions. This planning may further be complex by bringing multiple tasks simultaneously [93], [94]. The overall aim related to mission planning covers time efficiency, maximising material extrusion precision, and energy use efficiency. Future research will explore this optimisation type of mission planning solutions further [95].

While this study focuses upon pseudoplastic cementitious material development strategies and extrusion platform and nozzle considerations, in the current state of the AAM, two main materials have been printed using unmanned aerial vehicles (UAV) in self-powered, untethered flight within a laboratory environment: (i) cement-based mortar and paste; (ii) polyurethane foam-based material. For images and details of printed cement and foam structures using UAVs, the reader is referred to the AAM projects' UAV flight extrusion publication [38].

Considering future work, autonomy, end-effector precision and collective behaviour are the research nodes that should be undertaken for further advancement in aerial robotics. A swarm of UAVs should be able to coordinate work packages and flight paths without any collision or interference with a global digital twin, which is updated along with the material and built structure information and should be able to adapt and correct on the way for the most optimum and close result from the intended design. This necessitates a high level of autonomy with real-time scanning in the loop, higher precision at the tooltip, low platform vibration, greater payload capacity and flight endurance, and reduced disturbance from the flight dynamics with further software development for multi-agent coordination.

B. PRIORITISATION OF BUILDABILITY PHASE—DESIGN, RESULTS, AND DISCUSSION

Material extrusion experiments tested with the first 60 ml capacity deposition device focused upon buildability and

used both an 8 mm diameter circular nozzle, an aperture flush with the cartridge base (Fig. 3*u*) and 3D printed rectangular nozzles, fitted over the base of the cartridge (Fig. 3*s*) to confirm material suitability for both circular and rectangular nozzle designs.

1) MIX FORMULATION

A simple cement paste control mix without HEMC, termed mix *A*, with excellent workability but poor buildability [53], was used for comparison to the pseudoplastic mix developed for buildability, termed mix *B*, which focused upon the ability to immediately print from the deposition device on top of a previously extruded layer. In addition to pseudoplastic properties, HEMC was also added to the mix *B* to promote constituent binding and water retention, mitigating segregation within the deposition device. The proportions of each constituent in the mixes are illustrated in Fig. 6 in kg/m^3. Density of mix *A* was 2000 kg/m^3 and mix *B* 1700 kg/m^3. Plasticiser was added 1.5% by weight of binder to mix *A* and 1.0% to mix *B*. Water/binder ratios were 0.33 (*A*) and 0.47 (*B*), and the sand/binder ratio for mix *B* was 1.00.

2) TRAJECTORY DESIGN AND MANIPULATION

Examples of hand (rectangular filament) and robotic arm-driven (circular filament) printed objects using mix *B* are shown in Fig. 7. The material exhibits excellent buildability. Multiple layers in circular, sine-wave and curved formations, deposited immediately in succession upon completion of mixing, retain structure and definition following deposition. Robotic arm-controlled trajectories were programmed to ascend vertically to the next layer immediately following layer completion, resulting in a gap of 5 seconds between layer printing. The velocity of the robotic arm during extrusion was 3.3 mm/sec, the deposition device being the limiting factor rather than the arm itself or the material. A five-second gap was also left between layer deposition with the hand-printed specimens to allow the correct positioning of the cartridge for continuing deposition. The velocity of deposition was 10 mm/sec for hand movement.

3) TEST RESULTS

Fig. 8 shows calorimetric (Fig. 8*a*,*b*) and rheological results (Fig. 8*c*,*d*). It can be seen in the calorimetry images that less energy is transferred during the first 48 hours of the hydration process for mix *B* in relation to mix *A*. A time differential can also be observed in Fig. 8*b*, with a longer dormant period (Fig. 8*b* 2) and delayed calcium silicate hydrate (C-S-H) gel phase, and calcium hydroxide formation from C_3S, clearly occurring later in mix *B* (Fig. 8*b* 3). There is little difference observed in the later diffusion-limited reaction period (Fig. 8*b* 5). The rheology results reveal complex moduli for mix *B* to be higher than cement paste *A*, illustrating the buildability qualities of silica fume, sand and HEMC influencing the rigidity of mix *B*.

Fig. 9 shows SEM microstructural images of more angular, rough-surfaced sand particles (*a*), smoothed sand particles (Fig. 9*b*) and HEMC particles (Fig. 9*c*) (along with xanthan gum particles - Fig. 9*d* - used with the 310 ml capacity device and discussed further in section 7.3.5). Images illustrate how the surface of the smoother sand particles would aid workability (Fig. 9*b*), as opposed to the rougher, more uneven surface of the more typical building sand (Fig. 9*a*). The HEMC image (Fig. 9*c*) reveals highly irregular particle sizes and long polymer chains. HEMC performed successfully both in binding the constituents together (with segregation and compaction of material not in evidence) and increasing viscosity.

4) BUILDABILITY DISCUSSION

Although mix *B* contains less cement than mix *A*, it is suggested that Fig. 8*a*,b may also display confirmation that HEMC possesses secondary hydration-retarding properties, with mix *B* showing both a reduction in the energy transferred during the 48 hours following mixing (*a*) and the rate of transfer (*b*). The initial C_3A reaction leading to ettringite formation (Fig. 8*b* 1) appears to be unaffected, but the dormant period (Fig. 8*b* 2) is clearly extended. The rate of the C_3S reaction-led acceleration period (Fig. 8*b* 3), leading to the primary hydration products C-S-H gel and $Ca(OH)_2$, is reduced and formation of further ettringite and monosulfates from C_3A (Fig. 8*b* 4) appears less defined in mix *B*.

Three parameters affect the chemical structure of HEMC - the molecular weight, the presence of the hydroxyethyl group and the presence of the methoxyl group [66]. Hydroxyethyl cellulose (HEC) - without the methoxyl group - has been shown to retard both C_3A [96] and C_3S [97] hydration reactions. HEC reduces the rate of C_3A dissolution, ettringite precipitation and calcium hydroaluminate precipitation, with HEC particles adsorbed onto calcium hydroaluminate surfaces observed [96].

The presence of HEC leads to slower C_3S dissolution rates (dissolution is limited by the ionic composition of the liquid phase induced by the cellulose ether), strongly modifying the growth rate of the C-S-H gel phase. Through adsorption, cellulose ether restricts the nucleation and growth of C-S-H particles on surfaces of C_3S particles, which results in ultimately thicker, more permeable C-S-H shells [97]. HEMC has further been shown to retard the precipitation of calcium hydroxide (portlandite) [66].

Following the calorimetry results, further oscillation tests took place on the rheometer to assess the effectiveness of two accelerating admixtures in combating the retardation effects of HEMC: BASF Master X-seed 100 and a 1:1 laboratory-formulated combination of aluminium lactate and diethanolamine each added to mixes at a dosage of 3.25% by weight.

Master X-seed consists of a suspension of nano-sized crystalline C-S-H seeds and is designed to promote the rapid nucleation and growth of C-S-H crystals, primarily targeting

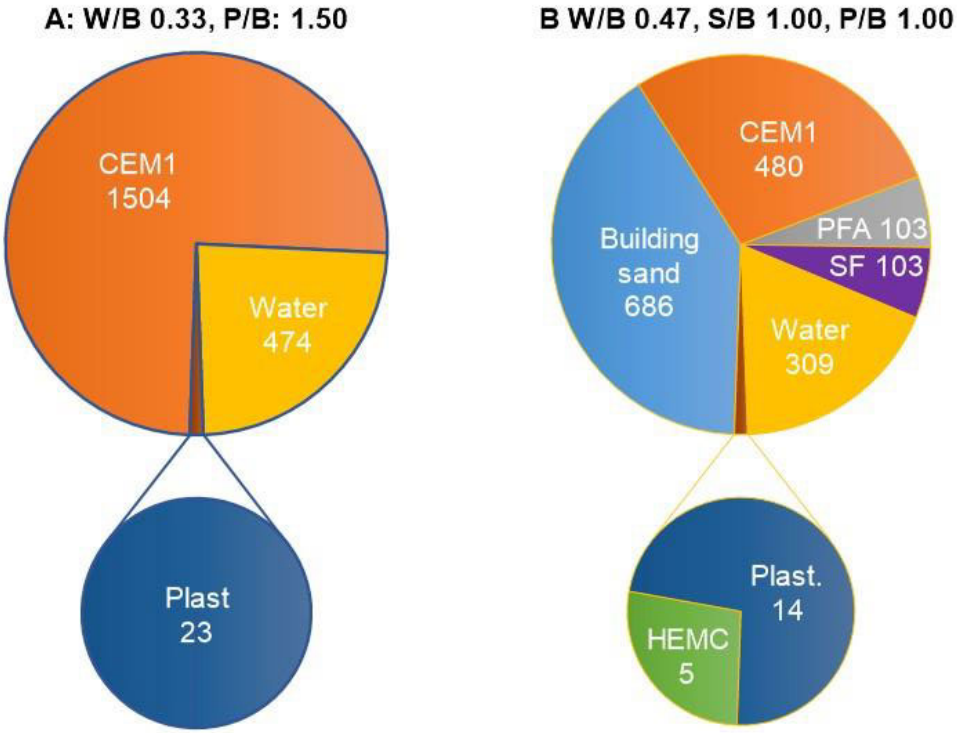

FIGURE 6. 60 ml capacity device mix formulations for AAM focused on buildability *B* and a cement paste control mix for comparison *A*. Constituent values are shown in kg/m^3. Fresh mix densities: *A*: 2000 kg/m^3, *B*: 1700 kg/m^3. Key: CEM I: Ordinary Portland cement type 1, PFA: pulverised fuel ash, SF: silica fume, Plast.: plasticiser, HEMC: hydroxyethyl methyl cellulose, W/B: water/binder Ratio, S/B: sand/binder Ratio. P/B: plasticiser/binder ratio.

the reduction of the dormant period following initial C_3A reactions [98]. However, in this study, the early stages of reactivity following mixing are of prime interest. Master X-seed did demonstrate an early accelerating influence with mixes showing increased G^*. However, considering practical use, a period following mixing completion has to be allowed for loading the material into a cartridge, placement of the cartridge into a deposition device, attachment of the deposition device to a UAV and allowing the UAV to manoeuvre into position before material can start flowing through the system and be extruded. This takes twenty minutes, and Master X-seed primarily achieves effect prior to this, suggesting that it would be inappropriate for AAM due to the risk of excessive stiffening occurring in the material while still in the deposition device before extrusion. Aluminium salt and diethanolamine forms an alkali-free accelerator designed to act upon aluminates, introducing a larger quantity of aluminium ions into the fresh mix to achieve acceleration [99] and promoting the quick formation of needle-like ettringite particles to stiffen the mix rapidly [100]. The presence of lactic acid in cement has been shown to accelerate aluminate phases rather than silicate phases [101]. Therefore, if cellulose ether inhibits the formation of hydration products arising from initial C_3A reactivity, aluminium lactate - diethanolamine ceases to be an effective accelerating solution and is inappropriate for AAM extrusion processes. Consequently, the strategy of this study to work with the open-time rheological properties of the fresh mix, rather than actively seeking to promote early hydration through the addition of acceleration agents, continued into the next phase.

The workability-buildability combination of mix *B* was appropriate for extrusion immediately out of the cartridge of this deposition device design. However, in readiness for fully testing mixes with flying UAVs, further experimentation was required, with workability being the primary parameter informing mix design, using a newly-developed, upscaled 310 ml cartridge device. The attachment of a deposition device to a UAV required a 560 mm length of flexible plastic tubing to connect the cartridge tip to a nozzle at the base of the UAV-attached delta robot, which controls the nozzle trajectory and stabilises movement. Mix *B* requires 800 N - 900 N of force to process mixes through the deposition devices' length of tubing. This proved too challenging for the power capabilities of the UAV batteries, which have to power both the UAV and the deposition device with a stabilising delta robot. Materials strategy, therefore, evolved to place extra importance on developing the pseudoplastic properties of the mixes, as viscosity is required to decrease by orders of magnitude while material passes through the deposition system, yet increase once deposited. While needing to exhibit liquid-like behaviour while in the deposition system, the

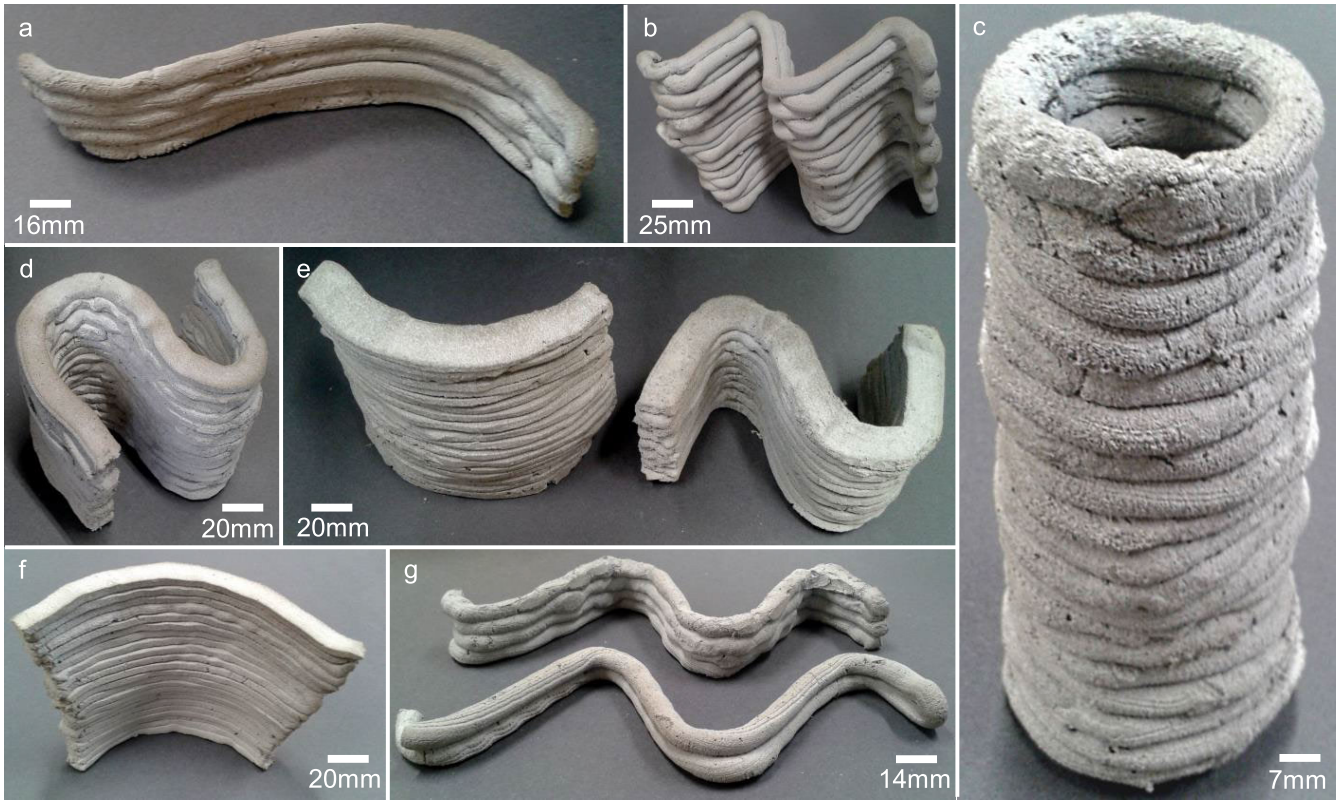

FIGURE 7. Hand and robotic arm-driven mix *B* extrusions using the 60 ml capacity device, using rectangular and circular nozzles, respectively. a) Partial sine wave with five layers. b) Sine wave, which shows variation in alternate layer trajectory. c) 20 circular layers deposited. d-f) Rectangular nozzle extrusions by hand. g) Sine wave extrusions using the robotic arm. Images *a-c* and *g* have 8 mm diameter circular extrusions. Images *d* and *f* feature a 15 mm wide and 5 mm high rectangular layer, with *e* having wider layers at 20 mm.

absence of added fast-acting acceleration agents means the material must also possess a yield stress sufficient to resist any impact from propeller downwash. If material does not possess suitable soft-solid behaviour, downwash risks deforming extruded material prior to curing, potentially leading to imperfections in the quality of the cured extruded filament and compromise the lateral precision of the resulting layer of material. In summary, this refinement in strategy placed extra importance upon the pseudoplastic behaviour of fresh material.

Fine aggregate should, therefore, consist of smoother particles of sand in a more workable mix. Rougher and more angular particles, along with wide variation in particle size, lead to increased viscosity as particles lock together in the fresh mix - an asset once extruded but a drawback pre-extrusion. Fine aggregate was also used in a reduced quantity, with increased use of pseudoplastic hydrocolloids to provide buildability.

C. PRIORITISATION OF WORKABILITY PHASE–DESIGN, RESULTS, AND DISCUSSION

During a further phase of experimentation focusing on workability, all mix designs were tested with the developed larger deposition device accommodating a larger 310 ml capacity cartridge. The flexible tubing which passes from the UAV deposition device cartridge through the stabilising delta robot arms was manipulated by hand during the material deposition tests detailed in this study.

1) MIX FORMULATION

Mix formulation involved increased use of smooth-particles PFA, decreased use of sand and investigation into whether alternative hydrocolloid constituents were superior, compatible or synergistic with HEMC. Table 5 lists the hydrocolloids investigated during the study to evaluate their effectiveness as an RMA suitable for AAM cementitious mixes. All hydrocolloids listed in Table 5 were trialled individually and with HEMC. Mix densities remained above 1700 kg/m^3.

Diutan gum is established as an RMA in concrete and cement [49], [102], [103]. However, during hydration, extruded mix formulations featuring diutan gum exhibited the behaviour of adsorbing water on the external surface of the material, giving a moist veneer to cured specimens - a behaviour not observed with the remaining hydrocolloids listed in Table 5. The anionic nature of diutan gum requires a polycarboxylate-based superplasticiser to prevent this surface adsorption [49]; therefore, diutan gum appeared to be

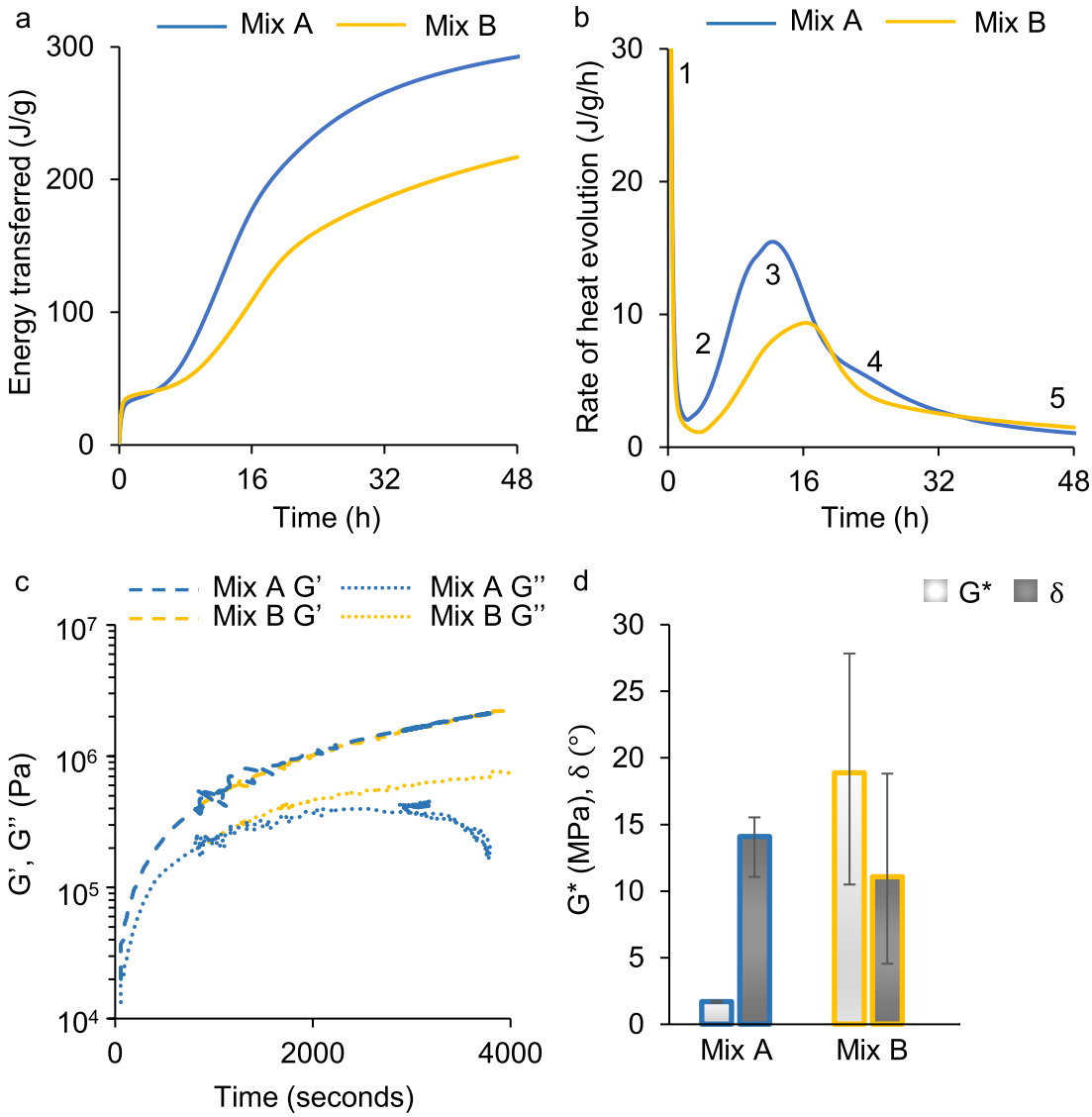

FIGURE 8. Rheology and calorimetry results for fresh 60 ml device mixes. a) Calorimetry - energy transferred during hydration for mixes *A* and *B*. b) Rate of heat evolution during hydration. 1: Initial C_3A reaction. 2: Dormant period. 3: Main C_3S reaction forming C-S-H gel and $Ca(OH)_2$. 4: Continuing C_3A reaction forming ettringite and monosulfates. 5: Diffusion limited reaction period. c) Oscillatory test results for mixes *A*, *B* and *C* showing elastic modulus *G′* and storage modulus *G″*. d) Complex modulus *G** and phase angle δ for mixes *A* and *B*.

incompatible with the lignin-based plasticiser used in this study.

In combination with HEMC, xanthan gum provided superior buildability in relation to the quantity used during trial formulations. Coupled with suitable workability, it was therefore decided that the most effective and AAM-appropriate rheological-modifying hydrocolloid was a combination of HEMC and xanthan gum, a hydrophilic native bio-polysaccharide derived from the bacteria xanthomonas campestris [104] following an aerobic fermentation process [60].

Three new mixes, termed *C* - *E*, were formulated (Fig. 10). Plasticiser content was maintained at 1% by weight of the binder. Constituents that promoted buildability, such as silica fume, were discontinued in the mix formulation.

2) TRAJECTORY DESIGN AND MANIPULATION

Fig. 11 illustrates extrusions with different trajectory designs using the hand-controlled 310 ml capacity device to demonstrate design possibilities using AAM.

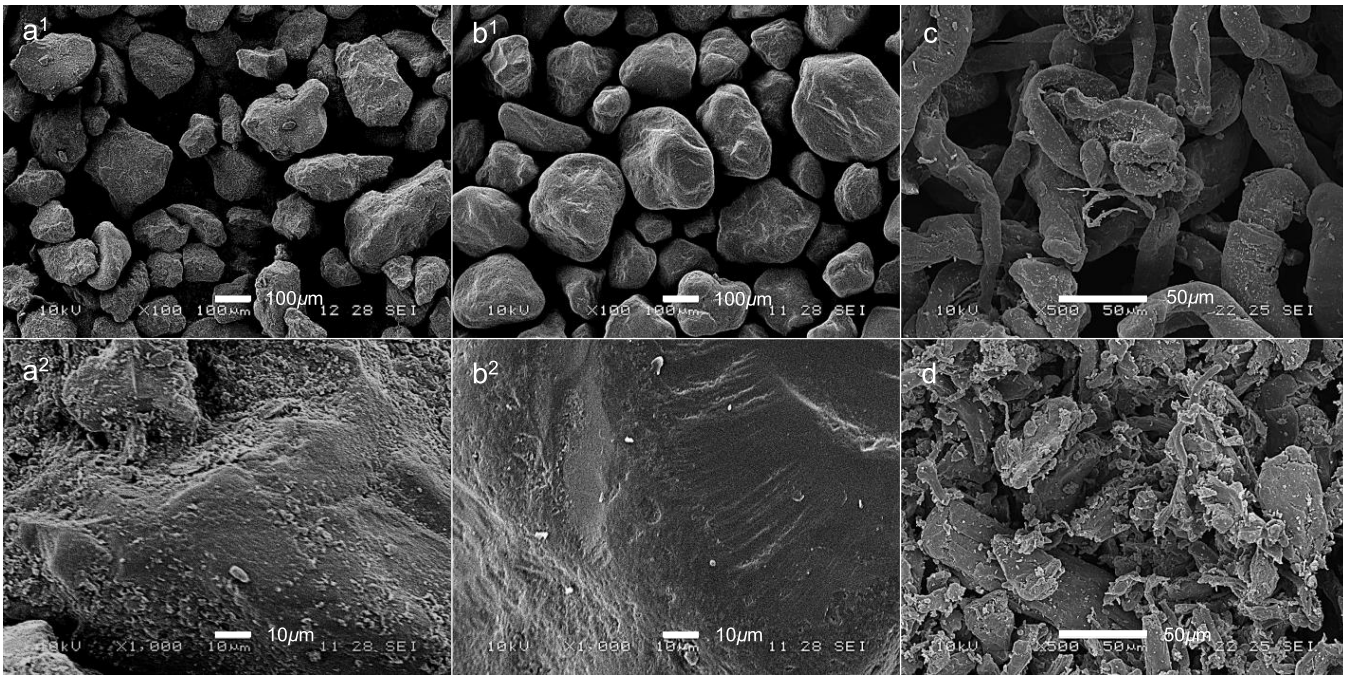

FIGURE 9. SEM images of fine aggregates and hydrocolloids: a) Building sand x100 (top) and x1000. b) Sports sand x100 (top) and x1000. c) HEMC x500. d) Xanthan gum x500.

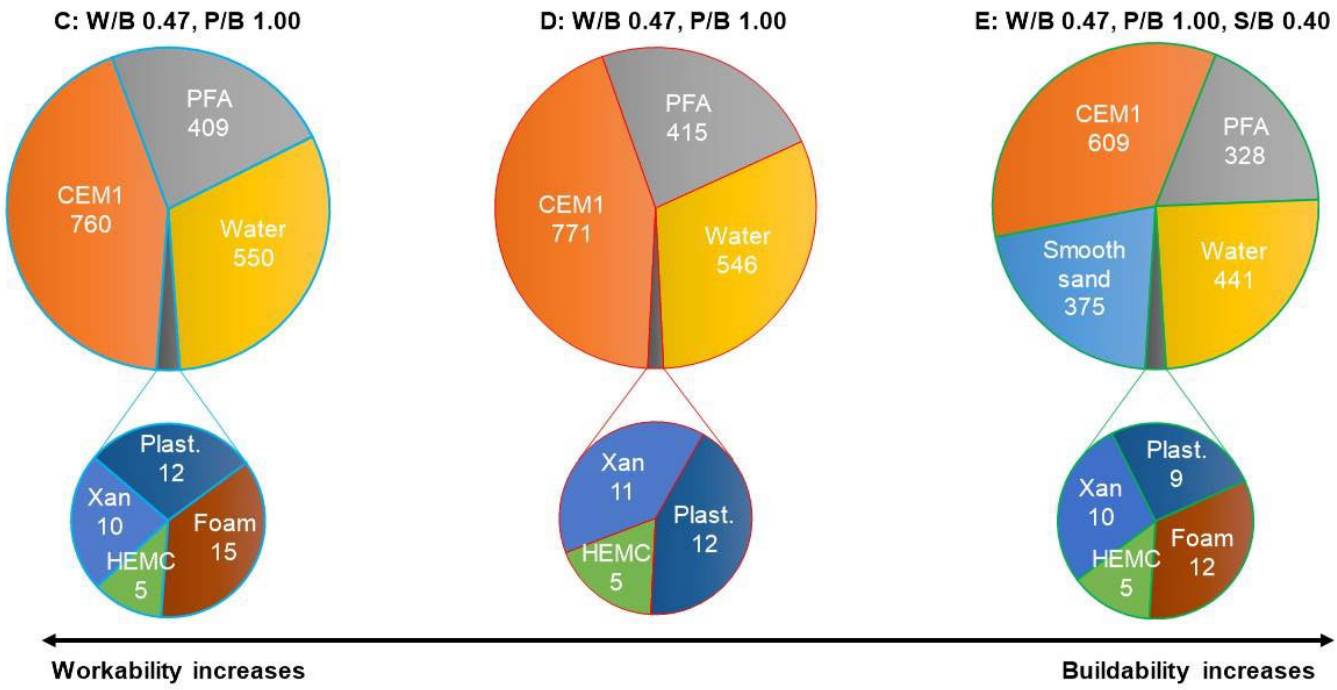

FIGURE 10. 310 ml capacity device mix formulations *C* - *E*, focusing upon workability. Constituent values are shown in kg/m^3. Fresh mix densities: *C*: 1760 kg/m^3, *D*: 1760 kg/m^3 *E*: 1790 kg/m^3. Key: CEM1: Ordinary Portland cement type 1, PFA: pulverised fuel ash, Plast.: plasticiser, HEMC: hydroxyethyl methyl cellulose, Xan=xanthan gum, W/B: water/binder Ratio, S/B: sand/binder Ratio, P/B: plasticiser/binder ratio.

An alternating ruffle and three orthogonal lines design can be seen in Fig. 11*a* in the form of a circular column and Fig. 11*b* in a more linear form. Fig. 11*c* shows a wall design with immediately adjacent extrusions, the alternating ruffle and line design, and a continuous curve style arrangement with alternating layers staggered in the centre-line circumference plane.

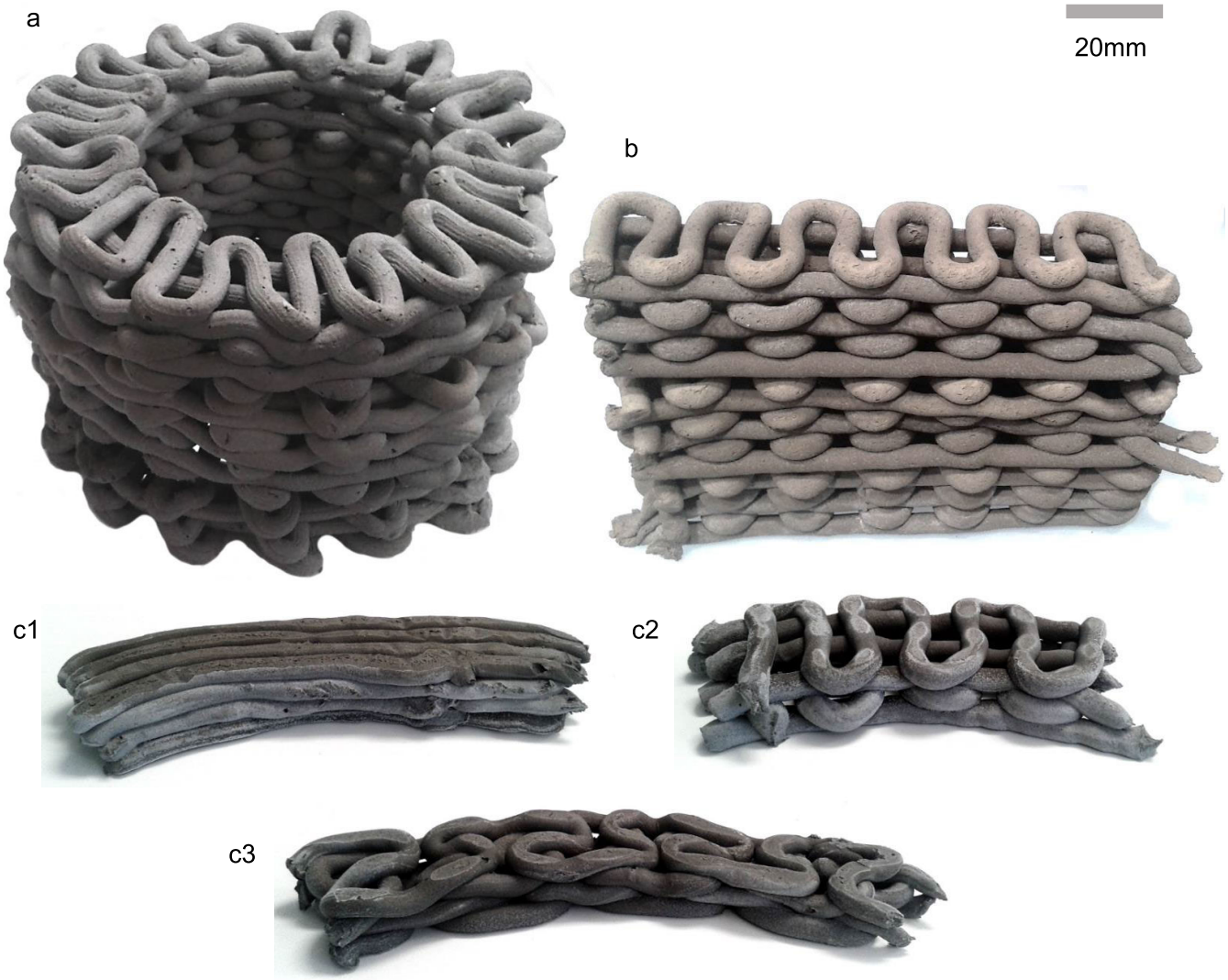

FIGURE 11. Extrusions using the 310 ml capacity device. a) Circular column element with alternating layers of three concentric lines and ruffle design featuring mixes *D* and *E* with the deposition device moved by hand. b) Examples with alternating layers of parallel lines and the ruffle design using mix *D*, with the deposition device moved by hand. c) Three designs printed by hand using mix *D*: Four adjacent beads forming a wall (c1), an alternating layer design using three straight lines alternating with a ruffle design (c2) and a continuous curve design (c3).

3) TEST RESULTS - MATERIAL DEFORMATION, AXIAL FORCE, POWER, RHEOLOGY AND CT

Freshly extruded mixes from the 310 ml capacity device demonstrated that mix *C* was the most workable but possessed inadequate buildability, while mix *E* showed suitable buildability (Fig. 11), but was the most challenging for the deposition device to print. Mix *D* displayed the best combination of workability and buildability (Fig. 11), with the deposition device being able to process the material more comfortably than mix *E* and once extruded, mix *D* material retains defined layers with less deformation than the more workable mix *C*.

Fig. 12 shows how mix *C* (workable paste) and mix *D* (buildable mortar) differed in settlement under loading (Mix *E* was similar to mix *D* and omitted for clarity). Deformation decreases for all four mixes as the material ages through the open time. Mix *C* exhibited greater deformation than mix *D* at the three different time stages illustrated - 10 minutes, 60 minutes and 110 minutes.

Force and current requirements increased as the material passed through the tubing and plateaued after extrusion had commenced. Fig. 13*a* shows the relationship between force and current for the mixes. Using equation (2) stresses experienced by the material are between 0.2 MPa - 0.4 MPa while in the cartridge, rising to 6 MPa - 13 MPa while in the tubing. Mixes *C* - *E* required less force to process than mixes *B* (which was ≈800 N) and *A* (≈900 N).

Fig. 13*b* depicts the two-hour oscillation test profile of the most suitable mix in this study for AAM deposition, mix *D*, showing how the elastic modulus *G*' dominates over the viscous modulus *G*'' for the pseudoplastic mortar mixes. Moduli values initially increase with the initial dissolution of

TABLE 5. Hydrocolloids investigated during AAM mix formulation.

Hydrocolloid	Manufacturer	Class	Typical applications
Hydroxyethyl methyl cellulose (HEMC)	Dow construction chemicals: Walocel VP-M-7701	Cellulose	Thickening and bonding agent in industrial paints, adhesives, grouts and dry-mix mortars
Carboxymethyl cellulose (CMC)	Classikool	Cellulose	Drilling-mud constituent and water binding agent in the oil industry
Xanthan	Minerals-water Ltd	Aerobic fermentation	Tertiary oil recovery, thickening agent in edible condiments
Guar	Minerals-water Ltd	Seed	Water binding agent in frozen foodstuffs
Diutan	CPKelco: Kelco-crete	Aerobic fermentation	Oil and construction industry cementitious RMA
Tragacanth	Classikool	Plant exudates	Stabiliser and thickener in creams, toothpastes and adhesives

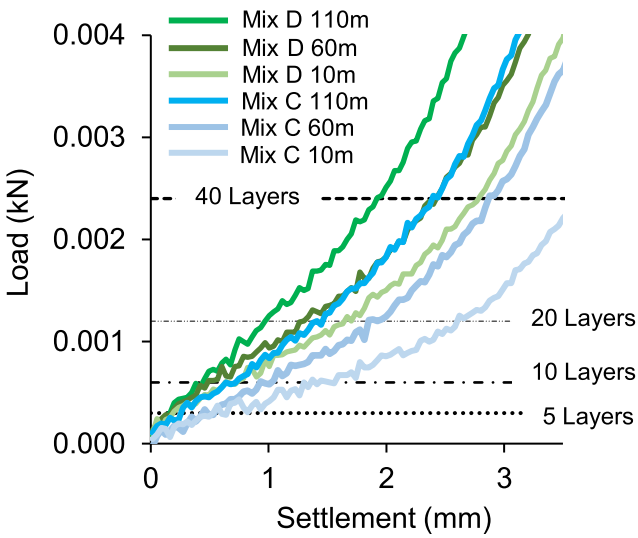

FIGURE 12. Deformation results for fresh 310 ml device mixes; settlement of mixes *C* and *D* under compressive loading (mix *E* was similar to mix *D* and omitted for clarity).

the C_3A phase and then broadly plateau for the remainder of the mix open time, within the dormant hydration period. Mixes in this study possessed a phase angle δ within the range of 3° - 10° and applying equation 4, complex moduli G^* can be calculated as 10^6 - 10^7 Pa. Therefore, 10 MPa can be considered a quantitative upper limit for AAM.

To quantitatively assess the optimisation of the 310 ml capacity device tubing dimensions concerning the resistance to flow imparted by the deposition device R and material viscosity η, Fig. 13*c* and Fig. 13*d* illustrate how the viscosity and resistance profiles for mix D would change in accordance with tubing dimension variation. Fig. 13*c*,d uses the viscosity profile of mix D, which shows viscosity reducing from 10^7 Pa.s while at rest to 10^2 Pa.s while moving through the length of tubing.

The current dimensions of the 310 ml capacity device tubing are indicated in Fig. 13*c*,d. The resistance profile (Fig. 13*c*) changes linearly with length yet begins to increase dramatically once radius values fall below 3 mm. With viscosity (Fig. 13*d*), increasing the tube radius beyond 4 mm sees the rate of viscosity increase significantly (with increases in orders of magnitude beyond 12 mm).

Fig. 14 shows the yield stress (*a*) and viscosity (*b*) flow curves for mixes C and D. Mix E was very similar to mix D and was omitted for clarity. It can be observed that the most suitable mix in this study, mix D, possesses a yield stress of 1.1 kPa, with mix C lacking sufficient buildability and displaying a lower yield stress. Viscosity decreases by orders of magnitude in all mixes, reducing to below 10 Pa.s as the shear rate increases.

Fig. 15 shows the 3D reconstruction of three wall trajectory designs - wall, ruffle and continuous curve. The multi-layered extruded specimens shown in the images were coated in a layer of dental plaster for the convenience of handling and having been subjected to mechanical tests. Extruded specimens can be viewed in 2D images from three planes, namely xy-plane, yz-plane, and zx-plane. The bright areas, which are grey colour, show the dense material in the part, such as cement and plaster, while the dark areas (black colour) represent pores and gaps in the extruded filaments. Pores may have originated from air bubbles during mix preparation. As shown in Fig. 15*a*, the wall structure deposited by mix D exhibit several pores and gaps in comparison with the other two structures. The three dark lines shown in Fig. 15*a* (1) suggest compromised layer-boundary bonding. However, it is surprising that no obvious layer-boundary gaps can be observed in the continuous curve specimen (shown in Fig. 15*c*), which was also deposited by using mix D. Thus, considering the inherent trajectory variation in hand-controlled extrusion, it is suggested that the different trajectory designs would affect the quality of the internal structures of deposited filaments. In terms of the alternating ruffle design (shown in Fig. 15*b*), the alternating layers of parallel lines and the ruffle design can be identified, which means the deposition structure was well maintained. A contributing factor to this is that mix E contained sand, which helps to provide a mix with buildability.

4) WORKABILITY DISCUSSION

A pseudoplastic material should possess low viscosity while in a miniature deposition system and experience as little flow resistance imparted by confining walls as possible. The results of this study have shown that tube radius is the key dimensional parameter when considering how a pseudoplastic material may pass through a miniature

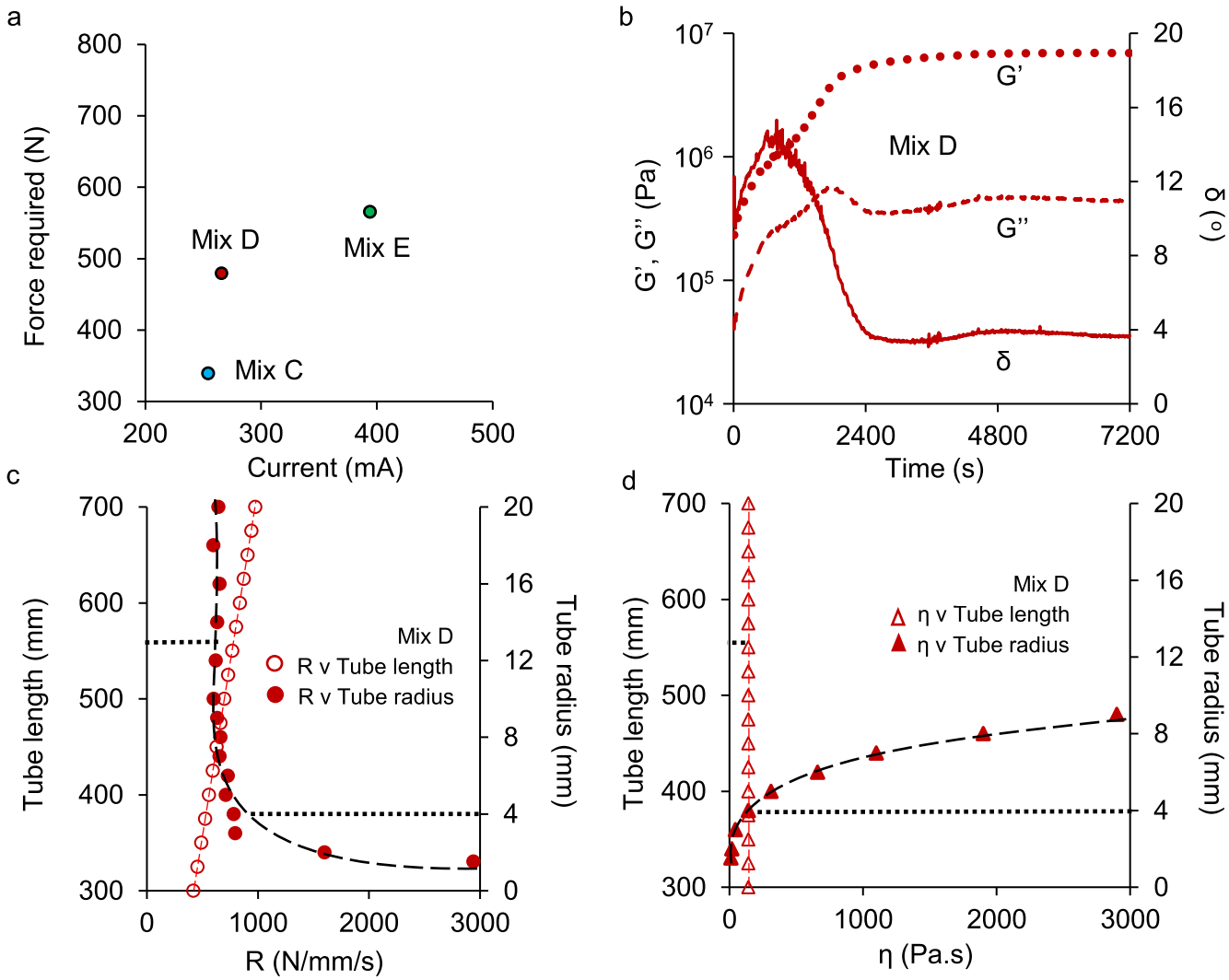

FIGURE 13. force, current required flow resistance and viscosity (in relation to deposition device cartridge and tubing dimensions) results for fresh 310 ml device mixes. a) Axial force and current required to process mixes through the tubing. b) Rheology oscillation test for mix *D*, which possessed the best workability-buildability combination, showing elastic modulus *G'*, viscous modulus *G''* and phase angle δ. c,d) Flow test for mix *D* showing the impact upon resistance to flow *R* and viscosity η that would arise from varying the tubing dimensions, demonstrating the suitability of the 560 mm length and 4 mm radius used in the extrusions.

deposition system. Tubing required to connect reservoir cartridge tips to extrusion nozzles is the component that exerts the most influence over material flow, and dimensional optimisation of tubing is of primary importance.

With a radius of 4 mm, resistance remains comparable to that imparted by a larger radius, and it is reasoned that the radius should not be reduced further. Increasing the radius beyond 4 mm would increase viscosity to a greater extent than reducing resistance. Therefore, a tubing radius of 4 mm is suggested to be optimal for a miniature deposition device suitable for AAM. Tubing length in this study is based on operational needs and the logistical necessity for the delta arm to function optimally; therefore, it cannot be reduced. Although length reduction would be beneficial, the results confirm length as the secondary parameter concerning pseudoplastic material flow within the device.

In the trial formulation, xanthan gum did not possess water-retentive and constituent binding qualities that were comparable to the standards exhibited by HEMC. It was also observed during trial mixes that HEMC in isolation did not impart such a strong influence over viscosity and yield stress compared to being combined with xanthan gum in equivalent quantities, though the effect was still pronounced. The two hydrocolloids proved synergistic in mixes, resulting in a cementitious-polymeric composite material suitable for AAM. With mix *D* exhibiting a yield stress of 1.1 kPa and possessing the most suitable workability-buildability combination in this study, it can be obtained that a material

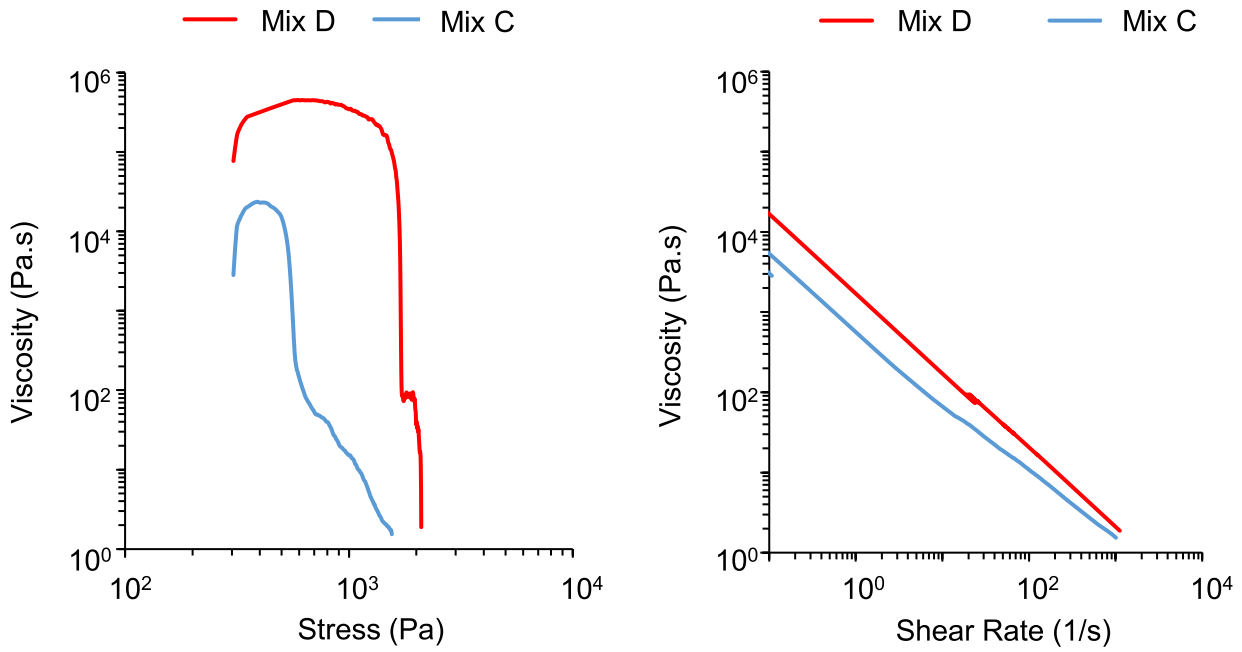

FIGURE 14. Yield stress (a) and viscosity (b) flow profiles shown for mixes *C* and *D*. (Mix *E* was very similar to mix *D* and is omitted for clarity).

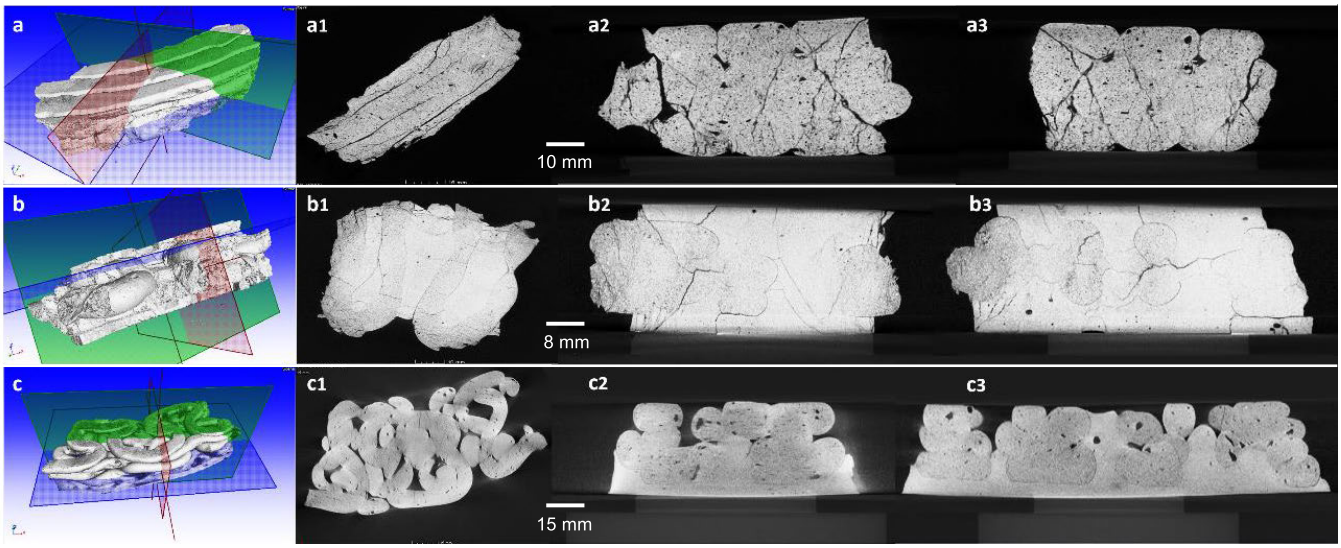

FIGURE 15. Micro-CT 3D images of a) a wall structure using mix *D*, b) a linear structure with alternating layers of parallel lines and the ruffle design using mix *E*, and c) a continuous curve using mix *D*. Their 2D image views are in xy-plane (1), yz-plane (2), and zx-plane (3), respectively.

suitable for a miniature automated deposition device should aim to possess neither significantly less (due to inadequate buildability) or significantly more, as mix *E* proved challenging for the deposition device and possessed only a marginal increased yield stress to mix *D*.

Although the SEM images (Fig. 9) support the choice of smooth-particle sand (rather than angular and sub-angular), the level of buildability provided by a sufficient quantity of the hydrocolloid combination can serve to reduce or eliminate the requirement for fine aggregate in a mix suitable for AAM. Therefore, the justification for using fine aggregate in these circumstances would be based on cost and carbon reductions rather than the necessity for buildability.

The HEMC micro-structural image (Fig. 9*c*) shows water-absorbing particles consisting of long polymeric chains capable of wrapping around water molecules, adsorbing and expanding, reducing segregation and bleeding in the fresh mix. Water-retaining HEMC particles also adsorb onto the surface of both C_3S and C_3A particles [97]. By contrast, the xanthan gum micro-structural image (Fig. 9*d*), shows

a greater particle distribution, with a greater quantity of smaller and more angular particles in comparison to HEMC, suggesting the ability to lock together, with smaller particles filling voids and increasing viscosity and buildability at low shear rates.

The two products affect viscosity by differing mechanisms - xanthan gum by adsorption onto cement particles, increasing inter-particle attraction, whereas HEMC molecules increase the viscosity of the water in the mix by adsorbing onto water molecules, expanding and attracting molecules in adjacent chains. Cellulose ether molecules entangle and intertwine amongst themselves at low shear rates, but at high shear rates, disentanglement and subsequent alignment parallel to flow direction occurs [61] - this pseudoplastic behaviour is desirable for AAM. Cellulose ether molecules additionally readily absorb moisture from the air [61].

HEMC and xanthan gum, a semi-synthetic hygroscopic polymer and a natural hydrophilic polymeric gum, respectively, are reasoned to be compatible and synergistic in fresh cementitious mixes suitable for AAM. This dual approach to increasing viscosity (at rest following extrusion) and decreasing viscosity (under stress within the deposition device) is particularly critical for a miniaturised deposition system.

The deformation results emphasise the importance of keeping spans to a minimum in trajectory design when working with mixes which adhere to the consideration of workability as being the primary parameter. A further course of action to address extruded bead deformation and promote hydration would be to investigate calcium aluminate cement (CAC) and calcium sulphate (CS) augmented mixes. Along with suitable plasticiser and alternative accelerating or retarding agents, this approach would be a means of controlling and promoting ettringite formation which promotes early rigidity (thus buildability) and strength.

The criteria of success for such an approach would be ideally to firstly provide sufficient open time for deposition device cartridge loading and subsequent UAV attachment and flight, plus a small buffer in case of a technical issue with the UAV operation. Following the expiration of the desired open time, which can be identified as a function of combined mix manufacture, deposition device loading and UAV flight time, a successful CAC/CS augmented system should promote rapid hydration, unhindered by the established retardation effects of HEMC.

The reader is referred to [38] for the demonstration that cementitious mixes can be extruded by a flying, self-powered untethered UAV to a lateral precision within 4 mm and cured material 28-day compressive strengths are shown to be in the region of ≈25 MPa; therefore AAM cementitious material is structurally viable. Considering the suitable rheological and structural properties of mixes containing a synergistic combination of pseudoplastic hydrocolloids, if the lateral in-flight trajectory deviation of the UAV is kept within 4 mm (set to decrease further through continuing iterative development), AAM with a miniature deposition device would be particularly suitable for precision repair work, especially at height. Considering the inherent dangers of working at height and on structures subjected to high lateral wind loading, this would be a prime application for AAM. UAVs are capable of landing upon vertical surfaces in addition to horizontal surfaces and an attached delta arm robot is capable of directing the nozzle administering the material in addition to stabilising UAV trajectories during flight.

Future work for novel AAM cementitious material development could examine whether any additional constituents may be added to further improve the compressive strength of cured material and minimise lateral deformation of extruded layers. However, additives and admixtures should not excessively compromise the workability or pseudoplastic properties of the material while in a fresh state and flowing through the deposition system. Alternative methods of accelerating fresh material may also be explored, such as CAC or another agent which may promote a flash-setting at the appropriate timescale shortly following deposition. Power capabilities of UAVs and the force imparted by custom extrusion mechanisms are also areas to continually evolve. These workflows should consider low energy usage, lightweight hardware characteristics, and versatility for different precision application scenarios while processing more viscous, denser cementitious material.

Additionally, AAM using UAVs would be an appropriate solution for repairing infrastructure cracks and potholes, such as those in roads and pavements, reducing the requirement for expensive labour and ground-based machinery in a sector where, in the developed world, repair expenditure can outstrip that of new infrastructure construction [105].

IV. CONCLUSION

This study demonstrated the feasibility of aerial additive manufacturing (AAM) and the development of a pseudoplastic cementitious-polymeric composite structurally viable material specifically for AAM. The material can be extruded by a lightweight miniature deposition system suitable to be carried and powered by an untethered unmanned aerial vehicle (UAV) in flight.

The study evaluated aerial platform considerations and identified differences between off-site ground-based additive manufacturing (AM) platforms and on-site aerial platforms, which highlighted the importance of maintaining stability and required the miniaturisation of the deposition process and development of pseudoplastic cementitious material for AAM, which were less dense than traditional or ground-based AM mortar mixes. Material approaches focused first on buildability, and as aerial platforms, deposition devices, extrusion tubing and nozzle requirements evolved, the need to ultimately focus on workability was emphasised.

Cementitious binders were CEM I-based, augmented by PFA and lignin-based plasticiser to aid workability. An effective rheology-modifying admixture was formed by combining hydroxyethyl methyl cellulose and xanthan gum. This combination is capable of mitigating constituent

segregation and providing sufficient material buildability for multiple-layer extrusion. Fine aggregate can be used in low ratios and should consist of sand particles with a smoothed surface and may be accompanied by a foaming agent to maintain sufficient workability. Material of 1700 kg/m^3 density is lightweight compared to traditional mortars. Important properties of fresh material suitable for AAM can be identified as 1.1 kPa yield stress, <10 MPa complex modulus, 4° phase angle, and requiring 500 N force and 250 mA current to be processed through the miniature deposition system. A parameter of key importance in the miniaturised deposition system is the circular cross-sectional area of tubing connecting a nozzle to the reservoir cartridge tip, with a 4 mm radius being identified as optimal for the miniature deposition device designed for on-site AAM deposition of cementitious material.

Any future work for material development could examine whether any further additives may be used to increase compressive strength of cured material or explore alternative methods of accelerating fresh material such as CAC. Continuing deposition device custom development could add increased power capabilities which in turn would allow an increase in viscosity and density of material. For aerial robotics, autonomy, end-effector precision and collective behaviour are areas identified for further advancement. Improvements in flight coordination necessitates continuing software development, a high level of autonomy with real-time scanning in the loop, higher precision at the tooltip, low platform vibration, increased payload capacity and flight endurance, and reduced disturbance from the flight dynamics.

AAM is a highly interdisciplinary fabrication technology. It comprehends aerial robotics, architectural design, and material science. The creation of cohesive cementitious structures with defined layers using AAM demonstrates a significant advancement towards bringing a high-precision on-site, multiple-agent, untethered aerial capability to AM in the construction industry.

ACKNOWLEDGMENT

The authors express thanks to the following: Dr. Ketao Zhang (automated deposition device development, Imperial College London, U.K., and Queen Mary University, London, U.K.); Dr. Pisak Chermprayong (Delta arm design development, Imperial College London, and Burapha University, Thailand); the Aerial Robotics Laboratory, Imperial College London, and the Laboratory of Sustainability Robotics, EMPA, Switzerland; William Bazeley and technical personnel of the Department of Architecture, the Civil Engineering Laboratories, University of Bath, U.K.; Philip Fletcher and Diana Lednitzky, Microscopy analysis suite, MC^2, University of Bath; Dow Chemical Company; EAB Associates; and CPkelco/BASF.

AUTHOR CONTRIBUTIONS

Conceptualization: Barrie Dams, Yusuf Furkan Kaya, Paul Shepherd, Mirko Kovac, and Richard J. Ball; Methodology: Barrie Dams, Binling Chen, Yusuf Furkan Kaya, Paul Shepherd, and Richard J. Ball; Software: Barrie Dams, Binling Chen, Yusuf Furkan Kaya, Lachlan Orr, Basaran Bahadir Kocer, Paul Shepherd, and Richard J. Ball; Validation: Barrie Dams, Binling Chen, Yusuf Furkan Kaya, Lachlan Orr, Basaran Bahadir Kocer, Paul Shepherd, and Richard J. Ball; Formal Analysis: Barrie Dams, Binling Chen, Yusuf Furkan Kaya, Lachlan Orr, and Basaran Bahadir Kocer; Investigation: Barrie Dams, Binling Chen, Yusuf Furkan Kaya, Lachlan Orr, and Basaran Bahadir Kocer; Resources: Barrie Dams, Binling Chen, Yusuf Furkan Kaya, Lachlan Orr, Basaran Bahadir Kocer, Paul Shepherd, and Richard J. Ball; Data Curation: Barrie Dams and Binling Chen; Writing—Original Draft Preparation: Barrie Dams, Binling Chen, Yusuf Furkan Kaya, Lachlan Orr, and Basaran Bahadir Kocer; Writing—Review and Editing: Barrie Dams, Binling Chen, Yusuf Furkan Kaya, Lachlan Orr, Basaran Bahadir Kocer, Paul Shepherd, Mirko Kovac, and Richard J. Ball; Visualization: Barrie Dams, Yusuf Furkan Kaya, and Binling Chen; Supervision: Paul Shepherd, Mirko Kovac, and Richard J. Ball; Project Administration: Barrie Dams, Paul Shepherd, Mirko Kovac, and Richard J. Ball; Funding Acquisition: Mirko Kovac and Richard J. Ball. All authors have read and agreed to the published version of the manuscript.

DATA AVAILABILITY

Data files supporting this paper are available from the University of Bath data archive at https://doi.org/10.15125/BATH-00693.

CONFLICTS OF INTEREST

The authors declare that they have no known competing financial interests or personal relationships that could have appeared to influence the work reported in this paper. The funding bodies has no role in the design of the study, in the collection, analysis, or interpretation of data, in the writing of the manuscript, or in the decision to publish the results.

NOTATIONS

The following notations are used in this manuscript and we selected a few units for clarification:

A	Cross sectional area of the cartridge
F	Axial force
G^*	Complex modulus
G'	Storage modulus
G''	Loss modulus
L	Length of the cartridge
MPa	MegaPascals
Q	Volumetric flow rate
r	Radius of the cartridge
R	Flow resistance

s	Seconds
V	Material flow velocity (mean)
V	Volts
δ	Phase angle
η	Viscosity of the material
σ	Compressive stress

ABBREVIATIONS

The following abbreviations are used in this manuscript:

AAM	Aerial Additive Manufacturing
AM	Additive Manufacturing
CAC	Calcium Aluminate Cement
CEM1	Ordinary Portland Cement type 1
CMC	Carboxymethyl Cellulose
CoG	Centre of Gravity
CS	Calcium Sulphate
CT	X-Ray Computed Tomography
DC	Direct Current
HEC	Hydroxyethyl Cellulose
HEMC	Hydroxyethyl Methyl Cellulose
LIDAR	Light Detection and Ranging
PFA	Pulverised Fuel Ash
RMA	Rheological Modifying Admixture
S/B	Sand/Binder ratio
SEM	Scanning Electron Microscopy
SLAM	Simultaneous Location And Mapping
UAV	Unmanned Aerial Vehicle
W/B	Water/Binder ratio

REFERENCES

[1] S. Lim, R. A. Buswell, P. J. Valentine, D. Piker, S. A. Austin, and X. De Kestelier, "Modelling curved-layered printing paths for fabricating large-scale construction components," *Additive Manuf.*, vol. 12, pp. 216–230, Oct. 2016.

[2] G. De Schutter, K. Lesage, V. Mechtcherine, V. N. Nerella, G. Habert, and I. Agusti-Juan, "Vision of 3D printing with concrete—Technical, economic and environmental potentials," *Cement Concrete Res.*, vol. 112, pp. 25–36, Oct. 2018.

[3] A. Pajonk, A. Prieto, U. Blum, and U. Knaack, "Multi-material additive manufacturing in architecture and construction: A review," *J. Building Eng.*, vol. 45, Jan. 2022, Art. no. 103603.

[4] T. Wangler, E. Lloret, L. Reiter, N. Hack, F. Gramazio, M. Kohler, M. Bernhard, B. Dillenburger, J. Buchli, N. Roussel, and R. Flatt, "Digital concrete: Opportunities and challenges," *RILEM Tech. Lett.*, vol. 1, pp. 67–75, Oct. 2016.

[5] J. M. Davila Delgado, L. Oyedele, A. Ajayi, L. Akanbi, O. Akinade, M. Bilal, and H. Owolabi, "Robotics and automated systems in construction: Understanding industry-specific challenges for adoption," *J. Building Eng.*, vol. 26, Nov. 2019, Art. no. 100868.

[6] Y. W. D. Tay, B. Panda, S. C. Paul, N. A. N. Mohamed, M. J. Tan, and K. F. Leong, "3D printing trends in building and construction industry: A review," *Virtual Phys. Prototyping*, vol. 12, no. 3, pp. 261–276, Jul. 2017.

[7] P. Carneau, R. Mesnil, N. Roussel, and O. Baverel, "Additive manufacturing of cantilever—From masonry to concrete 3D printing," *Autom. Construct.*, vol. 116, Aug. 2020, Art. no. 103184.

[8] A. Wolf, P. L. Rosendahl, and U. Knaack, "Additive manufacturing of clay and ceramic building components," *Autom. Construct.*, vol. 133, Jan. 2022, Art. no. 103956.

[9] V. Nguyen-Van, S. Li, J. Liu, K. Nguyen, and P. Tran, "Modelling of 3D concrete printing process: A perspective on material and structural simulations," *Additive Manuf.*, vol. 61, Jan. 2023, Art. no. 103333.

[10] N. Labonnote, A. Rønnquist, B. Manum, and P. Rüther, "Additive construction: State-of-the-art, challenges and opportunities," *Autom. Construct.*, vol. 72, pp. 347–366, Dec. 2016.

[11] J. Buchli, M. Giftthaler, N. Kumar, M. Lussi, T. Sandy, K. Dörfler, and N. Hack, "Digital in situ fabrication—Challenges and opportunities for robotic in situ fabrication in architecture, construction, and beyond," *Cement Concrete Res.*, vol. 112, pp. 66–75, Oct. 2018.

[12] R. A. Buswell, R. C. Soar, A. G. F. Gibb, and A. Thorpe, "Freeform construction: Mega-scale rapid manufacturing for construction," *Autom. Construct.*, vol. 16, no. 2, pp. 224–231, Mar. 2007.

[13] S. H. Ghaffar, J. Corker, and M. Fan, "Additive manufacturing technology and its implementation in construction as an eco-innovative solution," *Autom. Construct.*, vol. 93, pp. 1–11, Sep. 2018.

[14] D. G. Soltan and V. C. Li, "A self-reinforced cementitious composite for building-scale 3D printing," *Cement Concrete Compos.*, vol. 90, pp. 1–13, Jul. 2018.

[15] B. G. de Soto, I. Agustí-Juan, J. Hunhevicz, S. Joss, K. Graser, G. Habert, and B. T. Adey, "Productivity of digital fabrication in construction: Cost and time analysis of a robotically built wall," *Autom. Construction*, vol. 92, pp. 297–311, Aug. 2018.

[16] S. C. Paul, Y. W. D. Tay, B. Panda, and M. J. Tan, "Fresh and hardened properties of 3D printable cementitious materials for building and construction," *Arch. Civil Mech. Eng.*, vol. 18, no. 1, pp. 311–319, Jan. 2018.

[17] V. Richardson, "3D printing becomes concrete: Exploring the structural potential of concrete 3D printing," *Struct. Engineer*, vol. 95, no. 10, pp. 10–17, Oct. 2017.

[18] N. Melenbrink, J. Werfel, and A. Menges, "On-site autonomous construction robots: Towards unsupervised building," *Autom. Construct.*, vol. 119, Nov. 2020, Art. no. 103312.

[19] D. D. Camacho, P. Clayton, W. J. O'Brien, C. Seepersad, M. Juenger, R. Ferron, and S. Salamone, "Applications of additive manufacturing in the construction industry—A forward-looking review," *Autom. Construct.*, vol. 89, pp. 110–119, May 2018.

[20] E. Nadhim, C. Hon, B. Xia, I. Stewart, and D. Fang, "Falls from height in the construction industry: A critical review of the scientific literature," *Int. J. Environ. Res. Public Health*, vol. 13, no. 7, p. 638, Jun. 2016.

[21] T. S. Rushing, P. B. Stynoski, L. A. Barna, G. K. Al-Chaar, J. F. Burroughs, J. D. Shannon, M. A. Kreiger, and M. P. Case, "Investigation of concrete mixtures for additive construction," in *3D Concrete Printing Technology*, J. G. Sanjayan, A. Nazari, and B. Nematollahi, Eds. London, U.K.: Butterworth-Heinemann, 2019, ch. 7, pp. 137–160.

[22] T. T. Le, S. A. Austin, S. Lim, R. A. Buswell, A. G. F. Gibb, and T. Thorpe, "Mix design and fresh properties for high-performance printing concrete," *Mater. Struct.*, vol. 45, no. 8, pp. 1221–1232, Aug. 2012.

[23] I. Agustí-Juan, F. Müller, N. Hack, T. Wangler, and G. Habert, "Potential benefits of digital fabrication for complex structures: Environmental assessment of a robotically fabricated concrete wall," *J. Cleaner Prod.*, vol. 154, pp. 330–340, Jun. 2017.

[24] D. Marchon, S. Kawashima, H. Bessaies-Bey, S. Mantellato, and S. Ng, "Hydration and rheology control of concrete for digital fabrication: Potential admixtures and cement chemistry," *Cement Concrete Res.*, vol. 112, pp. 96–110, Oct. 2018.

[25] R. A. Buswell, A. Thorpe, R. C. Soar, and A. G. F. Gibb, "Design, data and process issues for mega-scale rapid manufacturing machines used for construction," *Autom. Construct.*, vol. 17, no. 8, pp. 923–929, Nov. 2008.

[26] D. Jiao, C. Shi, Q. Yuan, X. An, Y. Liu, and H. Li, "Effect of constituents on rheological properties of fresh concrete—A review," *Cement Concrete Compos.*, vol. 83, pp. 146–159, Oct. 2017.

[27] Y. Zhang, Y. Zhang, G. Liu, Y. Yang, M. Wu, and B. Pang, "Fresh properties of a novel 3D printing concrete ink," *Construct. Building Mater.*, vol. 174, pp. 263–271, Jun. 2018.

[28] D. P. Bentz, S. Z. Jones, I. R. Bentz, and M. A. Peltz, "Towards the formulation of robust and sustainable cementitious binders for 3D additive construction by extrusion," in *3D Concrete Printing Technology*, J. G. Sanjayan, A. Nazari, and B. Nematollahi, Eds. London, U.K.: Butterworth-Heinemann, 2019, ch. 15, pp. 307–331.

[29] S. Lim, R. A. Buswell, T. T. Le, S. A. Austin, A. G. F. Gibb, and T. Thorpe, "Developments in construction-scale additive manufacturing processes," *Autom. Construct.*, vol. 21, pp. 262–268, Jan. 2012.

[30] T. A. M. Salet, Z. Y. Ahmed, F. P. Bos, and H. L. M. Laagland, "Design of a 3D printed concrete bridge by testing," *Virtual Phys. Prototyping*, vol. 13, no. 3, pp. 222–236, Jul. 2018.

[31] S. J. Keating, J. C. Leland, L. Cai, and N. Oxman, "Toward site-specific and self-sufficient robotic fabrication on architectural scales," *Sci. Robot.*, vol. 2, no. 5, Apr. 2017, Art. no. eaam8986.

[32] I. Hager, A. Golonka, and R. Putanowicz, "3D printing of buildings and building components as the future of sustainable construction?" *Proc. Eng.*, vol. 151, pp. 292–299, 2016.

[33] P. Wu, J. Wang, and X. Wang, "A critical review of the use of 3-D printing in the construction industry," *Autom. Construction*, vol. 68, pp. 21–31, Aug. 2016.

[34] G. Hunt, F. Mitzalis, T. Alhinai, P. A. Hooper, and M. Kovac, "3D printing with flying robots," in *Proc. IEEE Int. Conf. Robot. Autom. (ICRA)*, May 2014, pp. 4493–4499.

[35] P. Shepherd and C. Williams, "Shell design considerations for 3D printing with drones," in *Proc. IASS Annu. Symp.* Madrid, Spain: International Association for Shell and Spatial Structures (IASS), 2017, pp. 1–10.

[36] B. Dams, S. Sareh, K. Zhang, P. Shepherd, M. Kovac, and R. J. Ball, "Aerial additive building manufacturing: Three-dimensional printing of polymer structures using drones," *Proc. Inst. Civil Eng. Construct. Mater.*, vol. 173, no. 1, pp. 3–14, 2020.

[37] B. Dams, "Cementitious and polymeric materials for aerial additive manufacturing," Ph.D. dissertation, Dept. Archit. Civil Eng., Univ. Bath, Bath, U.K., 2020.

[38] K. Zhang et al., "Aerial additive manufacturing with multiple autonomous robots," *Nature*, vol. 609, no. 7928, pp. 709–717, 7928.

[39] B. Khoshnevis, X. Yuan, B. Zahiri, J. Zhang, and B. Xia, "Construction by contour crafting using sulfur concrete with planetary applications," *Rapid Prototyping J.*, vol. 22, no. 5, pp. 848–856, Aug. 2016.

[40] J. Babel, "Up in the air: The emerging issue of drones in the construction industry," in *XL Catlin Construction Insider*, vol. 5. New York, NY, USA: XL Catlin, 2015.

[41] F. Augugliaro, S. Lupashin, M. Hamer, C. Male, M. Hehn, M. W. Mueller, J. S. Willmann, F. Gramazio, M. Kohler, and R. D'Andrea, "The flight assembled architecture installation: Cooperative construction with flying machines," *IEEE Control Syst. Mag.*, vol. 34, no. 4, pp. 46–64, Aug. 2014.

[42] Q. Lindsey, D. Mellinger, and V. Kumar, "Construction of cubic structures with quadrotor teams," in *Robotics: Science and Systems VII*, vol. 7. Cambridge, MA, USA: MIT Press, 2011.

[43] A. Braithwaite, T. Alhinai, M. Haas-Heger, E. McFarlane, and M. Kovač, "Tensile web construction and perching with nano aerial vehicles," in *Robotics Research*. Cham, Switzerland: Springer, 2018, pp. 71–88.

[44] A. Mirjan, F. Augugliaro, R. D'Andrea, F. Gramazio, and M. Kohler, "Building a bridge with flying robots," in *Robotic Fabrication in Architecture, Art and Design*. Cham, Switzerland: Springer, 2016, pp. 34–47.

[45] F. Augugliaro, E. Zarfati, A. Mirjan, and R. D'Andrea, "Knot-tying with flying machines for aerial construction," in *Proc. IEEE/RSJ Int. Conf. Intell. Robots Syst. (IROS)*, Sep. 2015, pp. 5917–5922.

[46] A. Mirjan, F. Gramazio, M. Kohler, F. Augugliaro, and R. D'Andrea, "Architectural fabrication of tensile structures with flying machines," in *Green Design, Materials and Manufacturing Processes*. London, U.K.: Taylor & Francis, 2013, pp. 513–518.

[47] S. Goessens, C. Mueller, and P. Latteur, "Feasibility study for drone-based masonry construction of real-scale structures," *Autom. Construction*, vol. 94, pp. 458–480, Oct. 2018.

[48] D. Wood, M. Yablonina, M. Aflalo, J. Chen, B. Tahanzadeh, and A. Menges, "Cyber physical macro material as a uav [re]configurable architectural system," in *Robotic Fabrication in Architecture, Art and Design*. Cham, Switzerland: Springer, 2018, pp. 320–335.

[49] M. Sonebi, "Rheological properties of grouts with viscosity modifying agents as diutan gum and welan gum incorporating pulverised fly ash," *Cement Concrete Res.*, vol. 36, no. 9, pp. 1609–1618, Sep. 2006.

[50] B. B. Kocer, M. E. Tiryaki, M. Pratama, T. Tjahjowidodo, and G. G. L. Seet, "Aerial robot control in close proximity to ceiling: A force estimation-based nonlinear MPC," in *Proc. IEEE/RSJ Int. Conf. Intell. Robots Syst. (IROS)*, Nov. 2019, pp. 2813–2819.

[51] A. Nettekoven and U. Topcu, "A 3D printing hexacopter: Design and demonstration," in *Proc. Int. Conf. Unmanned Aircr. Syst. (ICUAS)*, Jun. 2021, pp. 1472–1477.

[52] R. Mahony, V. Kumar, and P. Corke, "Multirotor aerial vehicles: Modeling, estimation, and control of quadrotor," *IEEE Robot. Autom. Mag.*, vol. 19, no. 3, pp. 20–32, Sep. 2012.

[53] B. Dams, Y. Wu, P. Shepherd, and R. Ball, "Aerial additive building manufacturing of 3D printed cementitious structures," in *Proc. 37th Cement Concrete Sci. Conf.*, 2017, pp. 345–348.

[54] B. Dams, K. Lumlerdwit, P. Shepherd, and R. Ball, "Fibrous cementitious material development for additive building manufacturing," in *Proc. IOMMM 38th Cement Concrete Sci. Conf.* Coventry, U.K.: Univ. Coventry, 2018, pp. 58–62.

[55] I. Müller, *Influence of Cellulose Ethers on the Kinetics of Early Portland Cement Hydration*. Karlsruhe, Germany: Universitätsverlag Karlsruhe, 2006.

[56] A. A. Hilal, "Microstructure of concrete," in *High Performance Concrete Technology and Applications*. London, U.K.: InTechOpen, 2016, pp. 3–24.

[57] N. Khalil, G. Aouad, K. El Cheikh, and S. Rémond, "Use of calcium sulfoaluminate cements for setting control of 3D-printing mortars," *Construction Building Mater.*, vol. 157, pp. 382–391, Dec. 2017.

[58] E.-A. Brujan, "Non-newtonian fluids," in *Cavitation in Non-Newtonian Fluids*. Heidelberg, Germany: Springer, 2011, pp. 1–47.

[59] S. Ross, "The inhibition of foaming. II. A mechanism for the rupture of liquid films by anti-foaming agents," *J. Phys. Colloid Chem.*, vol. 54, no. 3, pp. 429–436, Mar. 1950.

[60] P. de J. Cano-Barrita and F. León-Martínez, "Biopolymers with viscosity-enhancing properties for concrete," in *Biopolymers and Biotech Admixtures for Eco-Efficient Construction Materials*. Cambridge, U.K.: Woodhead, 2016, ch. 11, pp. 221–252.

[61] K. H. Khayat, "Viscosity-enhancing admixtures for cement-based materials—An overview," *Cement Concrete Compos.*, vol. 20, nos. 2–3, pp. 171–188, Jan. 1998.

[62] M. Sonebi and K. Khayat, "Effect of water velocity on performance of underwater, self-consolidating concrete," *Mater. J.*, vol. 96, no. 5, pp. 519–528, 1999.

[63] M. Sonebi and P. Bartos, "Hardened SCC and its bond with reinforcement," in *Proc. 1st Int. RILEM Symp.*, Stockholm, Sweden, Sep. 1999, pp. 275–289.

[64] D. Bülichen, J. Kainz, and J. Plank, "Working mechanism of methyl hydroxyethyl cellulose (MHEC) as water retention agent," *Cement Concrete Res.*, vol. 42, no. 7, pp. 953–959, Jul. 2012.

[65] G. Zhang, J. Zhao, P. Wang, and L. Xu, "Effect of HEMC on the early hydration of Portland cement highlighted by isothermal calorimetry," *J. Thermal Anal. Calorimetry*, vol. 119, no. 3, pp. 1833–1843, Mar. 2015.

[66] J. Pourchez, A. Peschard, P. Grosseau, R. Guyonnet, B. Guilhot, and F. Vallée, "HPMC and HEMC influence on cement hydration," *Cement Concrete Res.*, vol. 36, no. 2, pp. 288–294, Feb. 2006.

[67] P. Domone and J. Illston, *Construction Materials: Their Nature and Behaviour*. Boca Raton, FL, USA: CRC Press, 2010.

[68] D. Lootens, P. Hébraud, E. Lécolier, and H. Van Damme, "Gelation, shear-thinning and shear-thickening in cement slurries," *Oil Gas Sci. Technol.*, vol. 59, no. 1, pp. 31–40, Jan. 2004.

[69] T. Nawa, "Effect of chemical structure on steric stabilization of polycarboxylate-based superplasticizer," *J. Adv. Concrete Technol.*, vol. 4, no. 2, pp. 225–232, 2006.

[70] A. Kazemian, X. Yuan, E. Cochran, and B. Khoshnevis, "Cementitious materials for construction-scale 3D printing: Laboratory testing of fresh printing mixture," *Construct. Building Mater.*, vol. 145, pp. 639–647, Aug. 2017.

[71] B. B. Kocer, L. Orr, B. Stephens, Y. F. Kaya, T. Buzykina, A. Khan, and M. Kovac, "An intelligent aerial manipulator for wind turbine inspection and repair," in *Proc. UKACC 13th Int. Conf. Control (CONTROL)*, Apr. 2022, pp. 226–227.

[72] B. Stephens, L. Orr, B. B. Kocer, H.-N. Nguyen, and M. Kovac, "An aerial parallel manipulator with shared compliance," *IEEE Robot. Autom. Lett.*, vol. 7, no. 4, pp. 11902–11909, Oct. 2022.

[73] A. Suarez, F. Real, V. M. Vega, G. Heredia, A. Rodriguez-Castaño, and A. Ollero, "Compliant bimanual aerial manipulation: Standard and long reach configurations," *IEEE Access*, vol. 8, pp. 88844–88865, 2020.

[74] P. Zheng, X. Tan, B. B. Kocer, E. Yang, and M. Kovac, "TiltDrone: A fully-actuated tilting quadrotor platform," *IEEE Robot. Autom. Lett.*, vol. 5, no. 4, pp. 6845–6852, Oct. 2020.

[75] L. Orr, B. Stephens, B. B. Kocer, and M. Kovac, "A high payload aerial platform for infrastructure repair and manufacturing," in *Proc. Aerial Robotic Syst. Physically Interacting Environ. (AIRPHARO)*, Oct. 2021, pp. 1–6.

[76] F. Hauf, B. B. Kocer, A. Slatter, H.-N. Nguyen, O. Pang, R. Clark, E. Johns, and M. Kovac, "Learning tethered perching for aerial robots," in *Proc. IEEE Int. Conf. Robot. Autom. (ICRA)*, May 2023, pp. 1298–1304.

[77] M. Kishk, A. Bader, and M.-S. Alouini, "Aerial base station deployment in 6G cellular networks using tethered drones: The mobility and endurance tradeoff," *IEEE Veh. Technol. Mag.*, vol. 15, no. 4, pp. 103–111, Dec. 2020.

[78] V. Viswanathan, A. H. Epstein, Y.-M. Chiang, E. Takeuchi, M. Bradley, J. Langford, and M. Winter, "The challenges and opportunities of battery-powered flight," *Nature*, vol. 601, no. 7894, pp. 519–525, Jan. 2022.

[79] B. B. Kocer, V. Kumtepeli, T. Tjahjowidodo, M. Pratama, A. Tripathi, G. S. G. Lee, and Y. Wang, "UAV control in close proximities—Ceiling effect on battery lifetime," in *Proc. 2nd Int. Conf. Intell. Auto. Syst. (ICoIAS)*, Feb. 2019, pp. 193–197.

[80] (2023). *Aurelia X6 Standard*. Accessed: Feb. 3, 2023. [Online]. Available: https://aurelia-aerospace.com/product/aurelia-x6-standard/

[81] UAV. (2023). *Tarot 650 V2.2*. Accessed: Feb. 3, 2023. [Online]. Available: https://uavsystemsinternational.com/products/tarot-650-ready-to-fly-drone

[82] SwellPro. (2023). *Swelldrone Splashdrone 3+*. Accessed: Feb. 3, 2023. [Online]. Available: https://store.swellpro.com/products/splashdrone-3-waterproof-base-platform

[83] SwellPro. (2023). *SwellPro Fisherman*. Accessed: Feb. 3, 2023. [Online]. Available: https://swellpro-uk.co.uk/products/waterproof-fishing-drone-fd1

[84] Swellpro. (2023). *SplashDrone 4*. Accessed: Feb. 3, 2023. [Online]. Available: https://store.swellpro.com/products/splash-drone-4

[85] Dronevolt. (2023). *Hercules20*. Accessed: Feb. 3, 2023. [Online]. Available: https://www.dronevolt.com/en/expert-solutions/hercules-20/

[86] Dronevolt. (2023). *Hercules10*. Accessed: Feb. 3, 2023. [Online]. Available: https://www.dronevolt.com/en/expert-solutions/hercules-10/

[87] K. H. Petersen, N. Napp, R. Stuart-Smith, D. Rus, and M. Kovac, "A review of collective robotic construction," *Sci. Robot.*, vol. 4, no. 28, Mar. 2019, Art. no. eaau8479.

[88] R. Stuart-Smith, D. Darekar, P. Danahy, B. B. Kocer, V. Pawar, and M. Kovac, *Collective Aerial Additive Manufacturing: Incrementally Built Shell Structure Design*, M. Akbarzadeh, D. Aviv, H. Jamelle, and R. Stuart-Smith, Eds. Cambridge, U.K.: IngramSpark, 2023, pp. 44–55.

[89] L. J. Chen, J. Henawy, B. B. Kocer, and G. G. L. Seet, "Aerial robots on the way to underground: An experimental evaluation of VINS-mono on visual-inertial odometry camera," in *Proc. Int. Conf. Data Mining Workshops (ICDMW)*, Nov. 2019, pp. 91–96.

[90] J. Zhu, H. Zhou, Z. Wang, and S. Yang, "Improved multi-sensor fusion positioning system based on GNSS/LiDAR/vision/IMU with semi-tight coupling and graph optimization in GNSS challenging environments," *IEEE Access*, vol. 11, pp. 95711–95723, 2023.

[91] J. M. Aitken, M. H. Evans, R. Worley, S. Edwards, R. Zhang, T. Dodd, L. Mihaylova, and S. R. Anderson, "Simultaneous localization and mapping for inspection robots in water and sewer pipe networks: A review," *IEEE Access*, vol. 9, pp. 140173–140198, 2021.

[92] J. Sustarevas, D. Butters, M. Hammid, G. Dwyer, R. Stuart-Smith, and V. M. Pawar, "MAP—A mobile agile printer robot for on-site construction," in *Proc. IEEE/RSJ Int. Conf. Intell. Robots Syst. (IROS)*, Oct. 2018, pp. 2441–2448.

[93] M. Krizmancic, B. Arbanas, T. Petrovic, F. Petric, and S. Bogdan, "Cooperative aerial-ground multi-robot system for automated construction tasks," *IEEE Robot. Autom. Lett.*, vol. 5, no. 2, pp. 798–805, Apr. 2020.

[94] J. Sustarevas, K. X. Benjamin Tan, D. Gerber, R. Stuart-Smith, and V. M. Pawar, "YouWasps: Towards autonomous multi-robot mobile deposition for construction," in *Proc. IEEE/RSJ Int. Conf. Intell. Robots Syst. (IROS)*, Nov. 2019, pp. 2320–2327.

[95] J. P. Queralta, J. Taipalmaa, B. Can Pullinen, V. K. Sarker, T. N. Gia, H. Tenhunen, M. Gabbouj, J. Raitoharju, and T. Westerlund, "Collaborative multi-robot search and rescue: Planning, coordination, perception, and active vision," *IEEE Access*, vol. 8, pp. 191617–191643, 2020.

[96] J. Pourchez, P. Grosseau, and B. Ruot, "Current understanding of cellulose ethers impact on the hydration of C_3A and C_3A-sulphate systems," *Cement Concrete Res.*, vol. 39, no. 8, pp. 664–669, Aug. 2009.

[97] J. Pourchez, P. Grosseau, and B. Ruot, "Changes in C_3S hydration in the presence of cellulose ethers," *Cement Concrete Res.*, vol. 40, no. 2, pp. 179–188, Feb. 2010.

[98] *Master X-Seed 100—Hardening Accelerating Admixture for Concrete*, document EN 934-2, BASF, 2016.

[99] R. Myrdal, "Advanced cementitious materials—Controlling hydration development," SINTEF Building Infrastruct., COIN—Concrete Innov. Centre, Trondheim, Norway, Tech. Rep. SBF BK A07025, 2007, pp. 1–12.

[100] L. Reiter, T. Wangler, N. Roussel, and R. J. Flatt, "The role of early age structural build-up in digital fabrication with concrete," *Cement Concrete Res.*, vol. 112, pp. 86–95, Oct. 2018.

[101] N. B. Singh, S. Prabha, and A. K. Singh, "Effect of lactic acid on the hydration of Portland cement," *Cement Concrete Res.*, vol. 16, no. 4, pp. 545–553, Jul. 1986.

[102] L. Xu, H. Gong, M. Dong, and Y. Li, "Rheological properties and thickening mechanism of aqueous diutan gum solution: Effects of temperature and salts," *Carbohydrate Polym.*, vol. 132, pp. 620–629, Nov. 2015.

[103] M. Rubio, M. Sonebi, and S. Amziane, "3D printing of fibre cement-based materials: Fresh and rheological performances," *Academic J. Civil Eng.*, vol. 35, no. 2, pp. 480–488, 2017.

[104] J. A. Casas, A. F. Mohedano, and F. García-Ochoa, "Viscosity of guar gum and xanthan/guar gum mixture solutions," *J. Sci. Food Agricult.*, vol. 80, no. 12, pp. 1722–1727, 2000.

[105] V. C. Li and E. Herbert, "Robust self-healing concrete for sustainable infrastructure," *J. Adv. Concrete Technol.*, vol. 10, no. 6, pp. 207–218, 2012.

BARRIE DAMS is a Research Associate with the University of Bath, with a background in both civil engineering and finance. His research experience in academia has encompassed materials-based work, such as the use of materials for aerial additive manufacturing in the construction industry, such as cementitious pastes/mortar and polyurethane foams, along with structural engineering and building physics experience, with an emphasis on circular design within construction and the use of bio-based insulation materials in reversible wall systems. His current research work is focused on the history, behavior, and material properties of fibrous plaster ceilings and associated elements, such as wadding ties.

BINLING CHEN received the Ph.D. degree from the University of Exeter. Subsequently, he undertook a postdoctoral research with the University of Exeter. He is a Professor with the School of Mechanical Engineering, Beijing Institute of Technology, China. He also has a postdoctoral experience with the University of Bath prior to his return to China. He has long been engaged in research on additive manufacturing (3-D printing) of non-metallic materials and the manufacture of functional devices, with broad application prospects in the fields of construction, aerospace, environment, and energy. He has published a total of 45 SCI journal articles with three ESI highly cited papers.

YUSUF FURKAN KAYA is a Doctoral Researcher with the Aerial Robotics Laboratory, Imperial College London, in partnership with the Swiss Federal Laboratories for Materials Science and Technology (EMPA). Prior to research work, he has backgrounds in architecture and project management. His previous experience encompassed roles as a Junior Product Manager with Basler and Hofmann, Zürich, Switzerland; and as a junior Architect with Emre Arolat Architecture, London, U.K., and Folkart, Izmir, Turkey.

LACHLAN ORR received the bachelor's degree from Imperial College London. He is a Doctoral Researcher with the Aerial Robotics Laboratory, Imperial College London, in partnership with the Swiss Federal Laboratories for Materials Science and Technology (EMPA). His work on the Aerial Additive Manufacturing Project encompassed design development and flying of drones. His previous work experience encompassed working on a project with the Autonomous Manufacturing Laboratory, UCL at Here East, Stratford, London, during which a novel prototype quadcopter was developed for testing in the infra-red tracking arena.

BASARAN BAHADIR KOCER is a Lecturer with the University of Bristol. His research explores the integration of design, perception, and control in aerial robots; and investigating their impact on the operation and sustainable solutions for the future. His research focuses on aerial physical interaction for applications, including environmental sensing and aerial manufacturing and advance the eco-friendly and efficient use of aerial robots. Inspired by nature, he studied flexible and efficient learning schemes to develop designs, algorithms, and approaches, that can adapt to diverse aerial robots and tasks, an experience which informed his work on the aerial additive manufacturing work conducted with Imperial College London. He believes the emphasis on continuous learning enables us to tackle complex and dynamic challenges in aerial systems and the environment.

PAUL SHEPHERD is a Professor with the University of Bath. His research involves the development of new computer-based tools for both architects and engineers to help with the creation, optimization, and realization of complex geometry buildings. By combining mathematical techniques, such as dynamic relaxation, multi-objective optimization, and parametric modeling, he aims to facilitate the design of complex geometry forms, using computational techniques to improve the potential structural and environmental performance and constructability of the resulting shapes. He is confident that computers will become active participants in the design process and providing a common platform, on which design teams can interactively collaborate to create innovative and sustainable buildings.

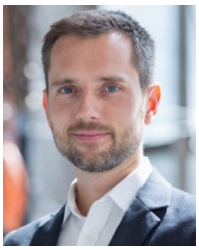

MIRKO KOVAC (Member, IEEE) is the Director of the Aerial Robotics Laboratory, Imperial College London; and the Head of the Materials and Technology Centre of Robotics, EMPA Material Science Institute, Switzerland. His research focuses on the development of novel, biologically inspired flying robots for distributed sensing in air and water, and on autonomous robotic construction for digital infrastructure systems. His particular specialization is in robot design, fluid-structure interaction, and multi-modal robot mobility. He is internationally known as an emerging leader in bio-inspired aerial robotics. He was the author of over 50 articles on mobile robotics that have been published in major journals, including *Science*, IEEE Transactions, and *Science Robotics*. He regularly advises industry, investment funds, and government on robotic research strategy. He is a holder of the prestigious Royal Society Wolfson Fellowship. He was a winner of multiple awards.

RICHARD J. BALL received the degree in materials science from the University of Bath. He worked on batteries, sensors, cements, photocatalytic materials, and indoor air quality. He currently holds the position of a reader with the university. His broad knowledge of materials has allowed him to focus on the development and performance of modern and historic construction materials. He has led multiple research projects funded by the Engineering and Physical Sciences Research Council concerning Additive Manufacturing, the Royal Society, the Royal Academy of Engineering, the Historic England, and the Leverhulme Trust. The projects have advanced the knowledge of important conservation materials, including lime mortars, nanolimes, and fibrous plaster.